BRAIN
A JOURNAL OF NEUROLOGY

CHP1 reduction ameliorates spinal muscular atrophy pathology by restoring calcineurin activity and endocytosis

Eva Janzen,[1] Natalia Mendoza-Ferreira,[1] Seyyedmohsen Hosseinibarkooie,[1] Svenja Schneider,[1] Kristina Hupperich,[1] Theresa Tschanz,[1] Vanessa Grysko,[1] Markus Riessland,[1,2] Matthias Hammerschmidt,[3,4] Frank Rigo,[5] C. Frank Bennett,[5] Min Jeong Kye,[1] Laura Torres-Benito[1] and Brunhilde Wirth[1,6]

Autosomal recessive spinal muscular atrophy (SMA), the leading genetic cause of infant lethality, is caused by homozygous loss of the survival motor neuron 1 (*SMN1*) gene. SMA disease severity inversely correlates with the number of *SMN2* copies, which in contrast to *SMN1*, mainly produce aberrantly spliced transcripts. Recently, the first SMA therapy based on antisense oligonucleotides correcting *SMN2* splicing, namely SPINRAZA™, has been approved. Nevertheless, in type I SMA-affected individuals—representing 60% of SMA patients—the elevated SMN level may still be insufficient to restore motor neuron function lifelong. Plastin 3 (PLS3) and neurocalcin delta (NCALD) are two SMN-independent protective modifiers identified in humans and proved to be effective across various SMA animal models. Both PLS3 overexpression and NCALD downregulation protect against SMA by restoring impaired endocytosis; however, the exact mechanism of this protection is largely unknown. Here, we identified calcineurin-like EF-hand protein 1 (CHP1) as a novel PLS3 interacting protein using a yeast-two-hybrid screen. Co-immunoprecipitation and pull-down assays confirmed a direct interaction between CHP1 and PLS3. Although CHP1 is ubiquitously present, it is particularly abundant in the central nervous system and at SMA-relevant sites including motor neuron growth cones and neuromuscular junctions. Strikingly, we found elevated CHP1 levels in SMA mice. Congruently, CHP1 downregulation restored impaired axonal growth in *Smn*-depleted NSC34 motor neuron-like cells, SMA zebrafish and primary murine SMA motor neurons. Most importantly, subcutaneous injection of low-dose SMN antisense oligonucleotide in pre-symptomatic mice doubled the survival rate of severely-affected SMA mice, while additional CHP1 reduction by genetic modification prolonged survival further by 1.6-fold. Moreover, CHP1 reduction further ameliorated SMA disease hallmarks including electrophysiological defects, smaller neuromuscular junction size, impaired maturity of neuromuscular junctions and smaller muscle fibre size compared to low-dose SMN antisense oligonucleotide alone. In NSC34 cells, *Chp1* knockdown tripled macropinocytosis whereas clathrin-mediated endocytosis remained unaffected. Importantly, *Chp1* knockdown restored macropinocytosis in *Smn*-depleted cells by elevating calcineurin phosphatase activity. CHP1 is an inhibitor of calcineurin, which collectively dephosphorylates proteins involved in endocytosis, and is therefore crucial in synaptic vesicle endocytosis. Indeed, we found marked hyperphosphorylation of dynamin 1 in SMA motor neurons, which was restored to control level by the heterozygous *Chp1* mutant allele. Taken together, we show that CHP1 is a novel SMA modifier that directly interacts with PLS3, and that CHP1 reduction ameliorates SMA pathology by counteracting impaired endocytosis. Most importantly, we demonstrate that CHP1 reduction is a promising SMN-independent therapeutic target for a combinatorial SMA therapy.

1 Institute of Human Genetics, Center for Molecular Medicine Cologne, Institute for Genetics, University of Cologne, Cologne, Germany
2 Laboratory of Molecular and Cellular Neuroscience, The Rockefeller University, New York, USA
3 Institute for Zoology, Developmental Biology, University of Cologne, Cologne, Germany

4 Cologne Excellence Cluster on Cellular Stress Responses in Aging Associated Diseases (CECAD), University of Cologne, Cologne, Germany
5 IONIS Pharmaceuticals, Carlsbad, USA
6 Center for Rare Diseases Cologne, University Hospital of Cologne, Cologne, Germany

Correspondence to: Prof. Dr Brunhilde Wirth
Institute of Human Genetics
University of Cologne
Kerpener Str. 34, 50931 Cologne
Germany
E-mail: brunhilde.wirth@uk-koeln.de

Introduction

Spinal muscular atrophy (SMA) is a devastating, common autosomal-recessive disorder with an incidence of 1 in 6000–10 000 and a carrier frequency of 1 in 35 in the European population and 1 in 54 worldwide (Feldkotter *et al.*, 2002; Sugarman *et al.*, 2012). SMA is mainly considered a motor neuron disorder since the disease hallmark is motor neuron loss in the anterior horns of the spinal cord leading to progressive muscle weakness and atrophy (Lunn and Wang, 2008). Strikingly, numerous studies in severely-affected SMA individuals and mice have shown additional non-neuronal organ impairments including heart, lung, intestine, pancreas, liver and bones. Therefore, SMA—at least in its severest form—should rather be considered a multi-systemic disorder (Hamilton and Gillingwater, 2013; Schreml *et al.*, 2013; Shababi *et al.*, 2014).

Homozygous deletions or mutations in the survival motor neuron 1 (*SMN1*) gene and insufficient functional SMN protein produced by the *SMN2* copy gene cause SMA (Lefebvre *et al.*, 1995). *SMN2* transcripts mainly lack exon 7 due to a translational silent variant disrupting an exonic splice enhancer creating a new splice silencer (Lorson *et al.*, 1999; Cartegni and Krainer, 2002; Kashima and Manley, 2003; Cartegni *et al.*, 2006). However, 10% of *SMN2* transcripts are correctly spliced and produce full-length protein identical to the one generated by *SMN1*. Consequently, in contrast to healthy individuals, all SMA individuals carry no functional *SMN1*, while the *SMN2* copy number inversely correlates with SMA severity (Feldkotter *et al.*, 2002; Wirth *et al.*, 2006). SMA1 (MIM: 253300) is the most severe and common form of the disease. These patients usually carry two *SMN2* copies, are never able to sit or walk unaided, and die within the first 2 years of life. SMA2 (MIM: 253550) is an intermediate SMA form; patients usually carry three *SMN2* copies and are able to sit but unable to walk. SMA3 (MIM: 253400) is considered a mild SMA form, patients typically have three to four *SMN2* copies and are able to sit and walk but often become wheelchair-bound later in life. SMA4 (MIM: 271150) is the adult form; affected individuals carry four to six *SMN2* copies, and mild motor disabilities start at >30 years of age (Lunn and Wang, 2008).

SMN is a housekeeping protein with essential functions in various cellular processes including snRNP biogenesis and splicing, microRNA biogenesis, transcription, and translation (Liu *et al.*, 1997; Pellizzoni *et al.*, 1998; Mourelatos *et al.*, 2002; Akten *et al.*, 2011). This essential role of SMN in all cell types explains the dysfunction of almost every organ in the severe forms of SMA. However, why motor neurons are particularly sensitive to reduced SMN levels and whether SMN displays a motor neuron specific function remains largely unknown.

Importantly, although various SMA modifiers have been identified by diverse screens in SMA animal models (Wirth *et al.*, 2017), plastin 3 (PLS3) overexpression and neurocalcin delta (NCALD) downregulation are the only human genetic protective modifiers of SMA, besides *SMN2* (Oprea *et al.*, 2008; Riessland *et al.*, 2017). Overexpression of the actin binding and bundling protein PLS3, as well as downregulation of the neuronal calcium sensor protein NCALD, protect individuals carrying a homozygous deletion of *SMN1* and only three or four *SMN2* copies, a genotypic combination usually causing SMA2 to SMA4. The protective effect of PLS3 overexpression and NCALD downregulation on the SMA phenotype has been demonstrated in various *in vitro* and *in vivo* SMA models, including mice, zebrafish, flies and nematodes (Oprea *et al.*, 2008; Dimitriadi *et al.*, 2010; Hao le *et al.*, 2012; Ackermann *et al.*, 2013; Hosseinibarkooie *et al.*, 2016; Kaifer *et al.*, 2017; Riessland *et al.*, 2017). Remarkably, the identification of PLS3 upregulation and NCALD reduction as SMA modifiers unveiled endocytosis, a process particularly important at neuromuscular junctions, as a key cellular mechanism impaired in SMA (Dimitriadi *et al.*, 2016; Hosseinibarkooie *et al.*, 2016; Riessland *et al.*, 2017).

Although the effect of PLS3-mediated protection has been widely studied, the molecular mechanism remains elusive. To unveil the mechanism behind the rescuing effect, we aimed to identify novel PLS3 interacting partners that could be

used to modify the disease phenotype and as potential therapeutic targets.

Here, we report the identification of calcineurin-like EF-hand protein 1 (CHP1) as a direct interacting partner of PLS3, show its protective effect in various *in vitro* and *in vivo* SMA models when it is downregulated, and unveil the molecular mechanism of protection underlying improved endocytosis. Most importantly, our study opens a new possibility for a combinatorial SMA therapy.

Material and methods

Yeast-two-hybrid screen

Full-length human *PLS3* cDNA (NM 005032.6) was cloned into the PBTG9 vector and used in a yeast-two-hybrid screen. Adult brain cDNA library (Clontech) was used as prey.

Co-immunoprecipitation and pull-down assay

For co-immunoprecipitation (Co-IP) experiments, HEK293T cells were co-transfected with Flag-His-PLS3 and CHP1-GFP expressing vectors. Cells were lysed in the respective immunoprecipitation lysis buffer, incubated with GFP-MicroBeads (Miltenyi Biotec) and added to the μ-columns. The μ-columns were washed with immunoprecipitation lysis buffer containing different Ca^{2+} concentrations (0, 0.1, 0.2, 0.3, 0.6 mM Ca^{2+}) and proteins were eluted with Laemmli buffer.

For pull-down assays, recombinant GST-CHP1 bound to the Glutathione HiCap Matrix (Qiagen) was incubated with His-PLS3 in pull-down buffer. After matrix washing, bound proteins were eluted with Laemmli buffer.

A detailed protocol is provided in the Supplementary material.

Immunostaining and western blotting

Immunofluorescent staining of cells and protein quantification by western blotting were performed according to standard protocols. A detailed description of antibodies used and respective dilutions are listed in the Supplementary material.

Short interfering RNA-mediated RNA silencing

For short interfering (si)RNA experiments, NSC34 (CLU140) cells were transfected with DharmaFECT 1 (ThermoFisher) according to the manufacturer's protocol. All siRNAs were purchased from Qiagen. SiRNA sequences: mmu-*Smn*: 5′-AAGAAGGAAAGTGCTCACATA-3′; mmu-*Chp1* 5′-TTCTTGCTTTCTAGTATTTAA-3′. AllStars Negative Control siRNA was used as control. Cells were harvested for protein isolation, fluorescence-activated cell sorting (FACS) or imaging, 48–72 h post-transfection. All experiments were performed in triplicate. Differentiation was induced with 1 μM retinoic acid 6 h post-transfection.

Calcineurin cellular activity assay

Cellular calcineurin phosphatase activity was measured using a complete colorimetric assay (Enzo). The assay was performed according to the manufacturer's protocol.

Endocytosis assay

NSC34 cells were starved for 2 h by serum depletion and incubated with 5 mg/ml fluorescein-isothiocyanate (FITC)-dextran (46945, Sigma) or 5 μg/ml transferrin (T13342, Invitrogen) during indicated time periods at 37°C. Subsequently, cells were washed with ice-cold phosphate-buffered saline (PBS), trypsinized (Trypsin, Sigma) and washed with PBS 1% bovine serum albumin (BSA). Fluorescence intensity was measured with FACSCalibur™ (BD Biosciences) and analysed with Cyflogic software (CyFlo Ltd.). Dead cells were excluded by propidium iodide staining (10 mg/ml, AppliChem). For inhibition studies, cells were treated for 30 min with 80 μM Dynasore (Abcam) or 10 μM cyclosporin A (Sigma) and subsequently incubated for 20 min with FITC-dextran.

Zebrafish experiments

Caudal primary motor neurons were analysed using the transgenic zebrafish line *tg(mnx1-GFP)*[ml2TG] (Synonym TL/EK-*hb9-GFP*; Flanagan-Steet *et al.*, 2005). All procedures were approved by LANUV NRW (reference number: 84-02.04.2012.A251). Morpholinos (MO) were purchased from GeneTools. *smn*-MO: 5′-CGACATCTTCTGCACCAT TGGC-3′, *chp1*-MO: 5′-CTGGAGCCCATGACTGCTGA AGATC-3′. Embryos at the 1–4-cell stage were injected into the yolk sac with 2 ng of *chp1* or *smn* morpholino separately or in combination and incubated at 28°C. To sort positively-injected eggs ~7 h post-fertilization (hpf), morpholinos were diluted in aqueous solution containing 0.05% Phenol Red and 0.05% rhodamine-dextran (Sigma). Zebrafish larvae were dechorionized ~34 hpf, fixed in 4% paraformaldehyde (PFA), permeabilized with 10 μg/ml proteinase K and blocked in PBS 0.1% Tween-20/1% DMSO (Sigma)/2% BSA/5% foetal calf serum. Embryos exhibiting morphological defects were excluded from analyses (Supplementary Fig. 3). To visualize motor axons, fish were stained with anti-Znp1 antibody and secondary α-Alexa Fluor® 488. For imaging, fish were laterally embedded in low-melting agarose slides. The first 10 motor axons after the yolk sac were quantified. Based on overall appearance, motor neurons were classified as: normal, short (truncated axonal projection) or atrophy (absent axonal projection) (Riessland *et al.*, 2017).

Mouse experiments

All mouse experiments were approved by LANUV NRW (reference number: 84-02.04.2014.A242). Taiwanese SMA mice [FVB.Cg-Tg(SMN2)2Hung Smn1tm1Hung/J, Stock Number 005058] (Hsieh-Li *et al.*, 2000) were purchased from Jackson Laboratory. Vacillator mice (B6.Cg-CHP1vac) (Liu *et al.*, 2013) were provided by Susan L. Ackerman, Howard Hughes Medical Institute and Jackson Laboratory, Bar Harbor, Maine. All mouse lines were backcrossed for seven generations to obtain a congenic C57BL/6 N background. Heterozygous $Chp1^{vac/wt}$ mice were crossed with $Smn^{ko/wt}$ mice to generate $Smn^{ko/wt}$; $Chp1^{vac/wt}$ mice. To obtain all required genotypes within one breeding, we crossed $Smn^{ko/wt}$; $Chp1^{vac/wt}$ with $Smn^{ko/wt}$; $SMN2^{tg/tg}$ mice (Fig. 4C). Genotyping for *Smn1*, *SMN2* and *Chp1* was performed as described (Ackermann *et al.*, 2013; Liu *et al.*, 2013).

Antisense oligonucleotide injection of mice

The offspring of the F1-generation (Fig. 4C) was subcutaneously injected with 30 μg of SMN antisense oligonucleotides (ASOs) (IONIS Pharmaceuticals) at postnatal Days 2 and 3 as described (Hua *et al.*, 2011; Hosseinibarkooie *et al.*, 2016).

Experimental design

According to the ARRIVE guidelines, all offspring of each litter were prior to SMN-ASO injection and processing randomized numbered by an independent person. The experimenter was blinded regarding genotypes of the mice at all steps until final statistical analysis. All experiments were performed at least in triplicates and blinded by randomized numbering by an independent person. To avoid pseudo-replication the mean value per animal and experiment was applied for statistical analysis.

Motoric tests

The righting reflex test was performed as previously described (El-Khodor *et al.*, 2008). Animals were tested between postnatal Days 3 and 12. Righting time scores were evaluated as following: 1 = 0–2 s; 2 = 3–4 s; 3 = 5–6 s; 4 = 7–8 s; 5 = 9–10 s; 6 = >10 s.

Motor coordination of vacillator mice was assessed using the beam-walking assay as previously described (Stanley *et al.*, 2005). After a short training period using a ruler (60 cm long, 3 cm wide, 30 cm elevated), three trials were performed for each mouse (50 cm long, 8 mm diameter, 30 cm elevated). The time to cross the beam was measured.

Compound muscle action potential and motor unit number estimation

Compound muscle action potential (CMAP) and motor unit number estimation (MUNE) were recorded as described (Arnold *et al.*, 2015; Bogdanik *et al.*, 2015). Mice were anaesthetized with inhaled isofluorane (5% induction, 1.5–2% maintenance and 1 l/min O_2 flow rate). Body temperature was maintained at 37°C with a thermostatic warming plate. Sciatic CMAP responses were recorded from the right hind limb using sensory needle electrodes (28 gauge, recording area active 2.0 mm^2). For recording, the active (E1) electrode was positioned subcutaneously at the proximal portion of the gastrocnemius muscle of the hind limb, at the knee joint. The reference electrode (E2) was placed at the metatarsal region of the foot of the same limb. For sciatic nerve stimulation at the proximal hind limb, two insulated 28 gauge (0.25 mm diameter) monopolar needle electrodes were placed subcutaneously over the sacrum (anode) and the sciatic notch (cathode). The sciatic nerve was stimulated with square-wave pulses of 0.1 ms duration and <10 mA intensity, until the responding amplitude no longer increased. Five repetitive CMAP responses were recorded for each mouse. The peak-to-peak amplitude of the CMAPs was measured (UltraPro S100, Natus Neurology). For MUNE, the initial incremental response and nine additional increments were recorded. MUNE was calculated as described (Arnold *et al.*, 2015).

Neuromuscular junction staining and quantification of size and maturity

Transversus abdominalis muscle was fixed for 20 min in 4% PFA and stained as described in standard immunohistochemistry protocols. The following primary antibodies were used: anti-SV2 and anti-NF-M for presynaptic and bungarotoxin Alexa Fluor® 555 for postsynaptic neuromuscular junction (NMJ) labelling. Quantification of NMJ size and maturity was performed using ImageJ (Riessland *et al.*, 2017). NMJ maturity was evaluated as followed: NMJs exhibiting ⩾3 perforations were evaluated as mature, NMJs with <3 perforations as immature (Bogdanik *et al.*, 2015).

Quantification of proprioceptive inputs

Sample preparation and analysis of proprioceptive inputs number per motor neuron soma was performed as previously described (Hosseinibarkooie *et al.*, 2016). The lumbar L4–L5 region of the spinal cord was used for quantifications. Primary anti-CHAT and anti-VGLUT1 antibodies and secondary Alexa Fluor® conjugated antibodies were used. Z-stacks of 30–50 slices (0.5 μm interval) were acquired. Proprioceptive inputs number and soma surface size were quantified using ImageJ.

Histology

Organ preparation and haematoxylin and eosin staining of paraffin sections of intestine and tibialis anterior muscle were performed as previously described (Ackermann *et al.*, 2013). Muscle fibre area was measured using ZEN software (Zeiss). For histological analysis of the cerebellum, anaesthetized mice (ketamine/xylazine: 0.1 ml/10 g) were fixed by transcardial perfusion with 4% PFA. Brains were incubated overnight in 4% PFA at 4°C and processed as described in standard protocols for paraffin sectioning. For colorimetric calbindin D-28 detection, anti-calbindin-D-28k antibody was used. Immunohistological stainings were performed as described in Storbeck *et al.* (2014) using an ABC kit (Vector Laboratories).

Primary cultures of motor neurons, hippocampal neurons and murine embryonic fibroblasts

Spinal cords and hippocampi were dissected from embryonic Day 12.5–13.5 and 16–18 mouse embryos, respectively, and processed for culture as previously described (Riessland *et al.*, 2017). Motor neurons and hippocampal neurons were plated on poly-D-lysine/laminin (Sigma, Invitrogen) and poly-D-lysine coated coverslips/plates, respectively. Neuronal culture medium was composed of Neurobasal® medium, B27 supplement, 2 mM L-glutamine, Pen/Strep (10 U/ml), and Amphotericin B (250 µg/ml) (Invitrogen). For motor neuron culture, Neurobasal® medium was supplemented with 2% horse serum, 10 ng/ml BDNF, 10 ng/ml GNTF, and 10 ng/ml CNTF (Peprotech). Primary murine embryonic fibroblasts (MEFs) were prepared from embryonic Day 12.5–13.5 animals as previously described (Ackermann *et al.*, 2013). Cells were grown under standard cell culture conditions (37°C, 5% CO_2).

Microscopy

Fluorescence images were acquired with a fully motorized fluorescence microscope AxioImager M2 (Zeiss) equipped with an ApoTome.2 system mimicking confocality (Zeiss). Zebrafish caudal primary motor neurons, as well as NMJs, spinal cord sections and MEF images were acquired as *z*-stacks. All quantitative measurements were performed using ZEN software (Zeiss) and ImageJ. For co-localization analysis the Pearson co-localization coefficient was determined using ImageJ with the plugin JACoP (Bolte and Cordelieres, 2006).

Statistical analysis

All statistical analyses were performed using the software programs Excel2013 (Microsoft), GraphPad Prism 6 and RStudio 1.1.442. Unpaired and paired two-tailed Student's *t*-test, for equal, and Welch's *t*-test, for unequal variances, were used for the comparison of two means. For multiple comparisons Holm correction was applied. Chi-square test was applied to compare frequencies of zebrafish motor axon categories. If not mentioned, all data are represented as mean ± standard error of the mean/standard deviation (SEM/SD). Mice survival was graphically represented by the Kaplan-Meier method and analysed applying log-rank test and exact Wilcoxon Rank test. Three levels of statistical significance were considered: *$P < 0.05$, **$P < 0.01$, and ***$P < 0.001$. Sample size for survival analysis was predetermined by Power analysis using G* Power 3.1 software. Exact *P*-values are listed in the Supplementary material. Note that N = number of individuals used, whereas n = number of replicates/similar objects tested in one and the same individual.

Results

CHP1 directly interacts with PLS3

To unveil the molecular pathomechanisms by which PLS3 acts as a protective SMA modifier, we searched for novel PLS3 interacting partners applying a yeast two-hybrid screen using human PLS3 as bait and a brain cDNA library as prey. CHP1 was the only identified interacting partner of PLS3 (Supplementary Fig. 1). To validate this result, we conducted detailed interaction studies of PLS3 and CHP1. HEK293T cells were co-transfected with CHP1-GFP and His-PLS3 expressing plasmids and co-immunoprecipitation studies were performed in the absence or presence of Ca^{2+}. Thereby, we proved that CHP1 and PLS3 are co-precipitating independently of Ca^{2+} (Fig. 1A). Furthermore, pull-down assays revealed that GST-CHP1 and His-PLS3 are directly interacting (Fig. 1B). Moreover, immunofluorescence analyses of MEFs isolated from PLS3-V5 overexpressing embryos (Ackermann *et al.*, 2013) showed that CHP1 and PLS3 strongly co-localize in filopodia (Fig. 1C). In congruence, the calculated correlation coefficient indicated a high linear correlation between PLS3 and CHP1 (Costes-adjusted Pearson coefficient 0.77). Together, these data support the fact that CHP1 is a novel direct interacting partner of PLS3.

CHP1 is highly abundant in neuronal tissue and elevated in SMA

The difference between expression patterns of two previously-identified SMA modifiers PLS3 (ubiquitously present) and NCALD (mainly restricted to neuronal tissues) explains the broader and stronger beneficial effect of PLS3 overexpression than NCALD reduction on the SMA phenotype (Hosseinibarkooie *et al.*, 2016; Riessland *et al.*, 2017). Therefore, we investigated CHP1 levels in various tissues from wild-type mice. CHP1 was present in all tested tissues, but was particularly abundant in neuronal tissues, including hippocampus, cortex, cerebellum and spinal cord (Fig. 2A). Next, we investigated the localization of CHP1 in motor neurons and NMJs by immunostaining. CHP1 showed a broad localization throughout the motor
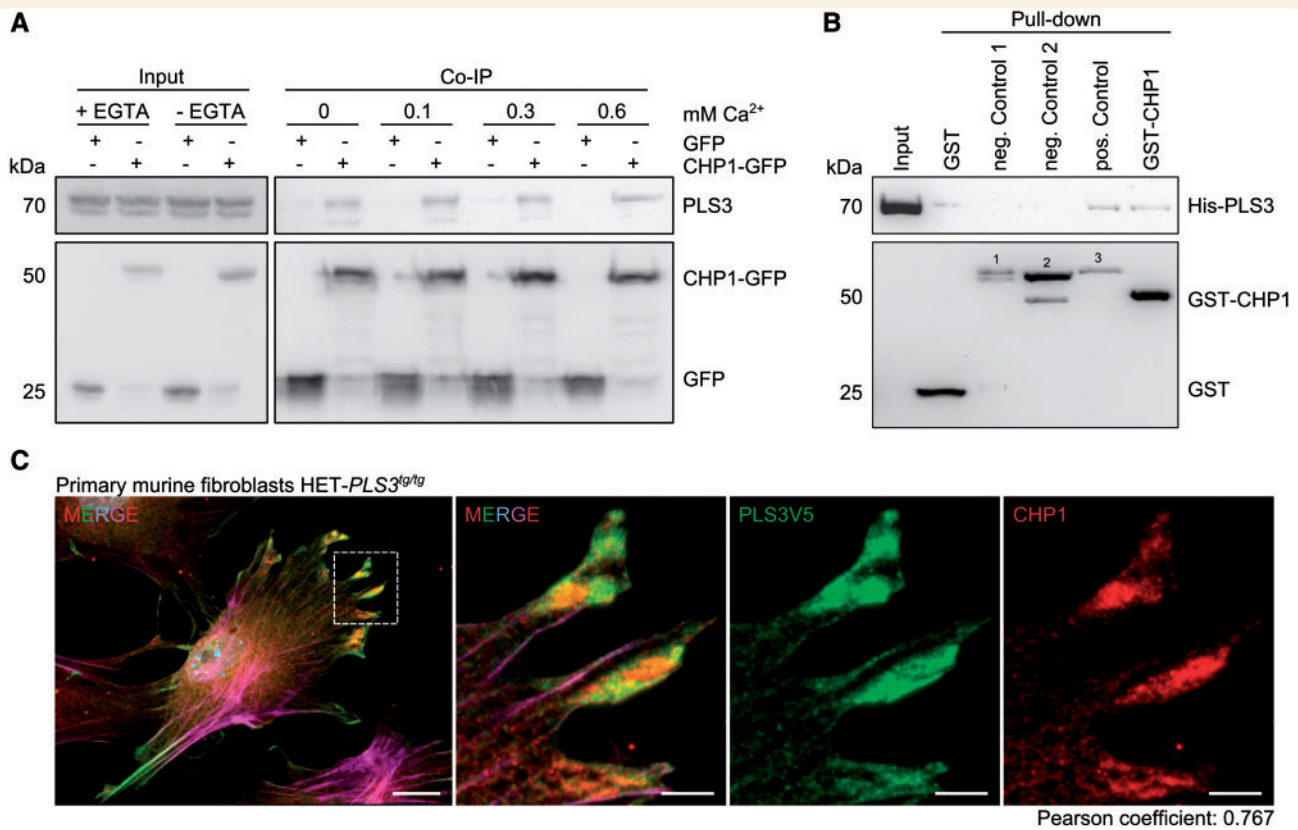
Figure 1 PLS3 and CHP1 are directly interacting. (**A**) Western blots of co-immunoprecipitation experiments show that CHP1 and PLS3 interact independently of Ca^{2+}. HEK293T were transiently co-transfected with CHP1-GFP and Flag-His-PLS3. Co-immunoprecipitation with GFP affinity microbeads revealed that CHP1 and PLS3 co-precipitate in the absence (addition of EGTA to the cell lysates) and presence of different Ca^{2+} concentrations. Input: total HEK293T cell lysates. PLS3 staining upper band: Flag-His-PLS3, lower band: endogenous PLS3. (**B**) Western blot of pull-down assay of purified GST-CHP1 (49 kDa) and His-PLS3 show that CHP1 and PLS3 directly interact. Input: purified His-PLS3 protein. Negative control 1: GST-CAPZA1 (59 kDa). Negative control 2: GST-CAPZB (58 kDa). Positive control: GST-hnRNPA1 (61 kDa) (Janzen, 2013). Numbers in blot: 1 = GST-CAPZA1; 2 = GST-CAPZB; and 3 = GST-hnRNPA1. (**C**) Co-localization analysis of CHP1 and PLS3V5 in HET-*PLS3V5*[tg/tg] transgenic MEFs. CHP1 and PLS3V5 co-localize in filopodia. α-CHP1 antibody (red), α-V5 antibody (green) for PLS3, phalloidin (magenta, for F-actin) and Hoechst (blue, for nuclei). Scale bars = 20 μm, *left*, inset magnifications = 5 μm. HET = heterozygous SMA (*Smn*[ko/wt]; *SMN2*[tg/0]).

neuron soma with the majority of CHP1 abundant in axon and growth cone (Fig. 2B, magnifications). For CHP1 localization analysis in NMJs, the transversus abdominis muscle, one of the most affected muscles in SMA (Murray *et al.*, 2008), was tested. A strong CHP1 localization along the axon and in the synapse at the NMJ was observed (Fig. 2C). Interestingly, CHP1, PLS3 and SMN display developmentally-related levels in spinal cord. SMN was highly abundant in mice at postnatal Days 7 and 14, and decreased over time, whereas the levels of both, CHP1 and PLS3, strongly increased between postnatal Days 7 and 14 (Fig. 2D and Supplementary Fig. 2). Strikingly, CHP1 level was elevated in spinal cord and brain of severely affected SMA (*Smn*[ko/ko]; *SMN2*[tg/0]) mice as compared to asymptomatic heterozygous SMA (HET) (*Smn*[ko/wt]; *SMN2*[tg/0]) mice used as controls (Fig. 2E and F), in contrast to no difference in PLS3 levels (Ackermann *et al.*, 2013). In summary, we confirmed the ubiquitous presence of CHP1, and showed that CHP1 is

particularly abundant in neuronal tissues and at SMA relevant sites including motor neuron soma and growth cone, and in the synapse of the NMJ. Furthermore, we demonstrate elevated CHP1 levels in severe SMA mice.

CHP1 reduction ameliorates SMA axonal outgrowth defects *in vitro* and *in vivo*

The SMA phenotype is mainly characterized by degeneration of motor neurons in anterior horns of the spinal cord, leading to progressive denervation and atrophy of skeletal muscles. Previous studies in NSC34 motor neuron-like cells showed a reduced neurite length upon *Smn* depletion (Nolle *et al.*, 2011). Since CHP1 is elevated in SMA, we next investigated whether *Chp1* knockdown can restore aberrant neurite outgrowth in *Smn*-depleted cells. Therefore, we differentiated NSC34 cells with retinoic acid for 72 h and measured the neurite length in the
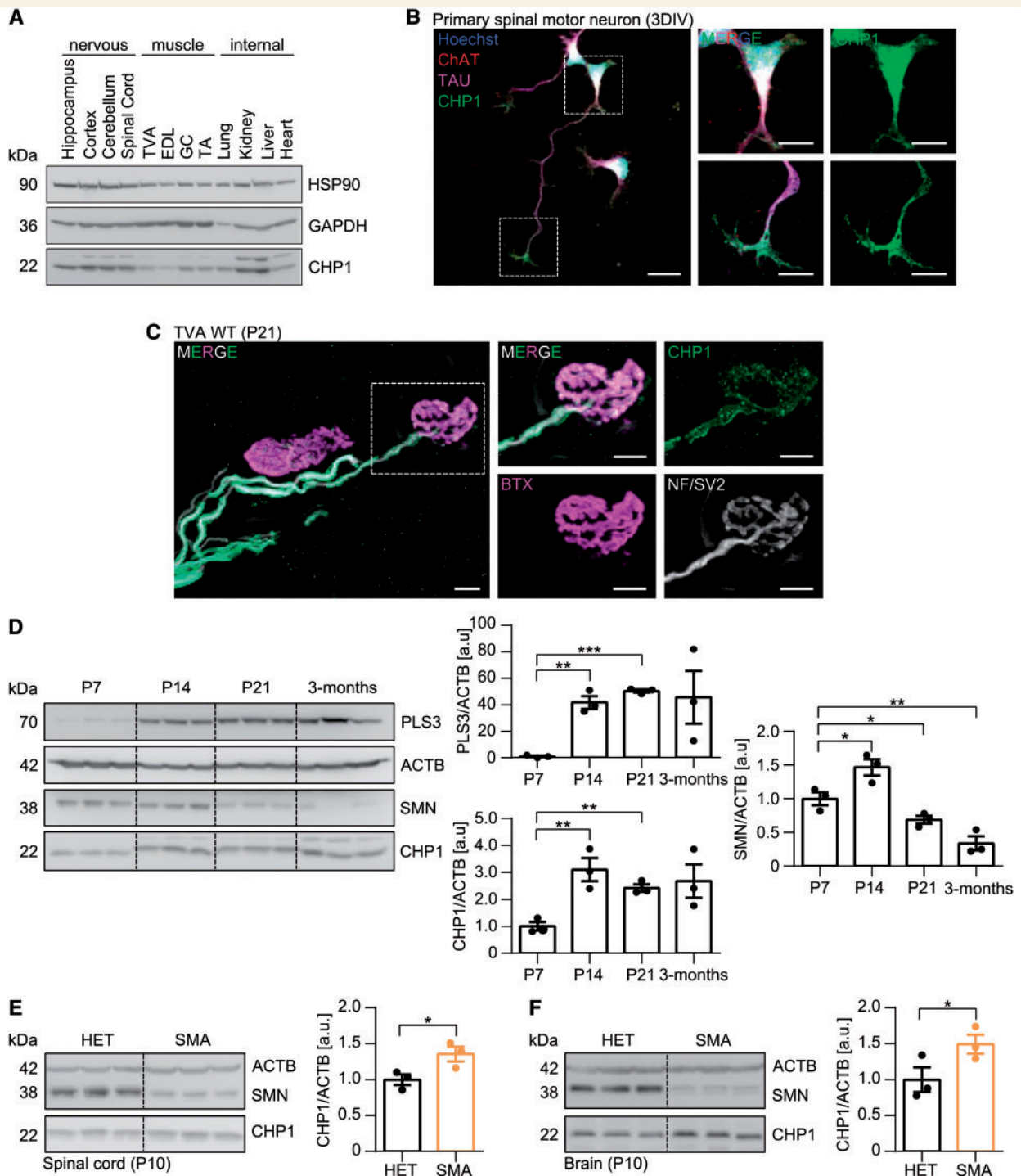
Figure 2 **CHP1 is abundant in motor neurons and shows increased level in spinal cord and brain derived from SMA mice.** (**A**) Western blots of protein lysates from different organs from a wild-type (WT) mouse at postnatal Day (P)10 show that CHP1 is ubiquitously expressed but especially abundant in neuronal tissues. EDL = extensor digitorum longus muscle; GC = gastrocnemius muscle; TA = tibialis anterior muscle; TVA = transversus abdominis muscle. GAPDH and HSP90 are loading controls. Wild-type mice were on congenic C57BL/6 N background. (**B**) CHP1 immunostaining of motor neurons at *in vitro* Day 3 isolated from wild-type embryonic Day (E)13.5 embryos show that CHP1 is broadly present in motor neurons. Scale bars = 20 µm; magnifications = 5 µm. High localization of CHP1 in motor neuron soma (*top*) and growth cone (*bottom*). (**C**) Immunostaining of CHP1 in wild-type transversus abdominis muscle at postnatal Day 21 indicates CHP1 localization in the synapse at the NMJ. α-CHP1 (green), α-bungarotoxin (BTX, magenta, for postsynapse), α-neurofilament (NF-M, white) and α-synaptic vesicle (SV2, white, for presynapse). Scale bars = 10 µm; inset magnifications = 10 µm. (**D**) Western blot analysis of PLS3, CHP1, SMN and ACTB (loading control) in spinal cord of wild-type mice at postnatal Days 7, 14, 21 and at 3 months. CHP1 and PLS3 levels markedly increase between postnatal Days 7 and 14, while SMN levels decrease after postnatal Day 14 ($N = 3$). Unpaired two-tailed Student's *t*-test compared to postnatal Day 7, *$P < 0.05$, **$P < 0.01$, and ***$P < 0.001$. Error bars represent SEM. (**E**) Increased CHP1 level in spinal cord and (**F**) brain derived from SMA mice as compared to heterozygous (HET) ($Smn^{ko/wt}$; $SMN2^{tg/0}$) mice. Western blot analysis of CHP1, SMN and ACTB (loading control) in spinal cord HET ($Smn^{ko/wt}$; $SMN2^{tg/0}$) and SMA ($Smn^{ko/ko}$; $SMN2^{tg/0}$) mice at postnatal Day 10 ($N = 3$). *$P < 0.05$, unpaired two-tailed Student's *t*-test. Error bars represent SEM.

different knockdown conditions. Knockdown efficiency was confirmed by western blotting (Fig. 3A). Consistent with previous results, a significant decreased neurite length in *Smn*-depleted cells was observed, which was fully restored to control levels by *Chp1* knockdown (Fig. 3B). Instead, overexpression of CHP1-GFP resulted in shorter neurites (Supplementary Fig. 4A), strengthening the hypothesis, that CHP1 levels influence neurite outgrowth. In line with this, we observed increased motor neuron axon length in *Chp1* mutant mice, presenting very low CHP1 amounts (Supplementary Fig. 4B).

Next, we investigated the effect of Chp1 suppression *in vivo* in zebrafish. Human CHP1 and its zebrafish orthologue are 90% identical. Moreover, Chp1 is highly abundant in primary motor neurons (Supplementary Fig. 4C). Hence, we performed a morpholino (MO)-mediated knockdown of either *smn* or *chp1*, or both in zebrafish embryos. Knockdown efficiency was confirmed by western blotting (Fig. 3D). The specificity of both morpholinos has been previously proven by rescue experiments with wild-type *SMN* or wild-type *CHP1* mRNA (McWhorter *et al.*, 2003; Mendoza-Ferreira *et al.*, 2018). In line with earlier studies, *smn* depletion resulted in motor axon outgrowth defects and altered axon morphology (Fig. 3C) (McWhorter *et al.*, 2003). Importantly, combined *smn* and *chp1* depletion significantly ameliorated motor axon outgrowth defects (Fig. 3C and E). Thus, we demonstrate that CHP1 reduction not only ameliorates the axonal phenotype of SMA *in vitro* but also *in vivo* in an SMA zebrafish model.

## CHP1 reduction ameliorates the SMA phenotype in mice

Next, we analysed the influence of CHP1 reduction in a severe and intermediate SMA mouse model. The intermediate mouse model was generated by injection of low-dose SMN-ASO into a severe SMA mouse model on C57BL/6N background (Hosseinibarkooie *et al.*, 2016). Additionally, we used a genetically modified *Chp1*-deficient mouse model (named 'vacillator'), carrying a splice site mutation (Liu *et al.*, 2013). Homozygous *Chp1* ($Chp1^{vac/vac}$) mice hardly show any CHP1 protein, whereas heterozygous ($Chp1^{vac/wt}$) mice show a ~50% reduction of CHP1 in spinal cord, primary motor neurons and cerebellum (Fig. 4A, B and Supplementary Fig. 5A). Homozygous $Chp1^{vac/vac}$ mice or biallelic mutated individuals develop autosomal recessive inherited cerebellar ataxia; instead individuals with heterozygous *CHP1* mutation or heterozygous $Chp1^{vac/wt}$ mice are asymptomatic (Liu *et al.*, 2013; Mendoza-Ferreira *et al.*, 2018). $Chp1^{vac/wt}$ mice show neither an ataxic gait nor Purkinje cell loss (Supplementary Fig. 5B and C). To generate SMA mice carrying a heterozygous *Chp1* mutation, we applied the depicted breeding strategy (Fig. 4C). Our previous studies showed that neither transgenic *PLS3* overexpression nor heterozygous *Ncald*

knockout in a severely-affected SMA mouse model prolonged survival due to the massive multi-organ dysfunctions of dramatically reduced SMN level; similar results were obtained for CHP1 (Fig. 4D and E). Instead, slightly increased SMN levels by injecting low-dose SMN-ASOs provided an adequate intermediate SMA phenotype (Hosseinibarkooie *et al.*, 2016; Riessland *et al.*, 2017). Pre-symptomatic subcutaneous injection of low-dose SMN-ASO at postnatal Days 2 and 3 prolonged median survival from 16 days to 26 days (Fig. 4D and E) by ameliorating inner organ impairment (Supplementary Fig. 6B). Low-dose SMN-ASO injection elevated SMN levels in liver but not in spinal cord (Fig. 4F) and CHP1 reduction did not influence SMN-ASO activity (Supplementary Fig. 6A). Remarkably, additional CHP1 reduction in SMA-$Chp1^{vac/wt}$ + ASO mice further significantly prolonged median survival form 26 days to 29 days, while mean survival was prolonged from 31.15 ± 15 to 51.95 ± 39 days (Fig. 4D and E). Moreover, weight progression analysis demonstrated a trend towards increased body weight of SMA-$Chp1^{vac/wt}$ + ASO mice (Fig. 4G). Previous studies reported a decreased CMAP as well as a reduced MUNE in SMA (Arnold *et al.*, 2015; Bogdanik *et al.*, 2015). Symptomatic SMA + ASO-treated mice showed a strongly reduced CMAP response and a diminished MUNE at postnatal Day 21, which were both ameliorated upon CHP1 reduction (Fig. 4H and I). Pre-symptomatic testing of the motoric abilities by righting reflex test—a test sensitive in non-treated severe SMA mice up to 2 weeks (El-Khodor *et al.*, 2008)—did not reveal any difference between genotypes (Supplementary Fig. 6C). Taken together, we show that CHP1 reduction not only prolongs survival of low-dose SMN-ASO-injected severe SMA mice but also ameliorates electrophysiological defects found in SMA.

CHP1 reduction restores axonal outgrowth, neuromuscular junction size and maturation in SMA mice

Finally, we tested the influence of reduced CHP1 levels on well-described hallmarks of SMA pathology in mice, including defects in axonal outgrowth, proprioceptive inputs on motor neuron soma, NMJ size and maturation as well as muscle fibre size (Kariya *et al.*, 2008; Murray *et al.*, 2008; Kong *et al.*, 2009; Mentis *et al.*, 2011; Bogdanik *et al.*, 2015).

Immunostainings of primary motor neuron cultures showed a significantly shorter axon length in SMA compared to HET motor neurons at Day 5 *in vitro*, which was fully restored by heterozygous *Chp1* mutation (Fig. 5A) and thus comparable to our previous results in *Smn*-depleted NSC34 cells and zebrafish (Fig. 3B and E). Next, we quantified the motor neuron surface area and number of proprioceptive inputs per motor neuron in spinal cord (L4–5) cross sections of SMN-ASO-injected mice at postnatal Day 21. SMA + ASO mice displayed a
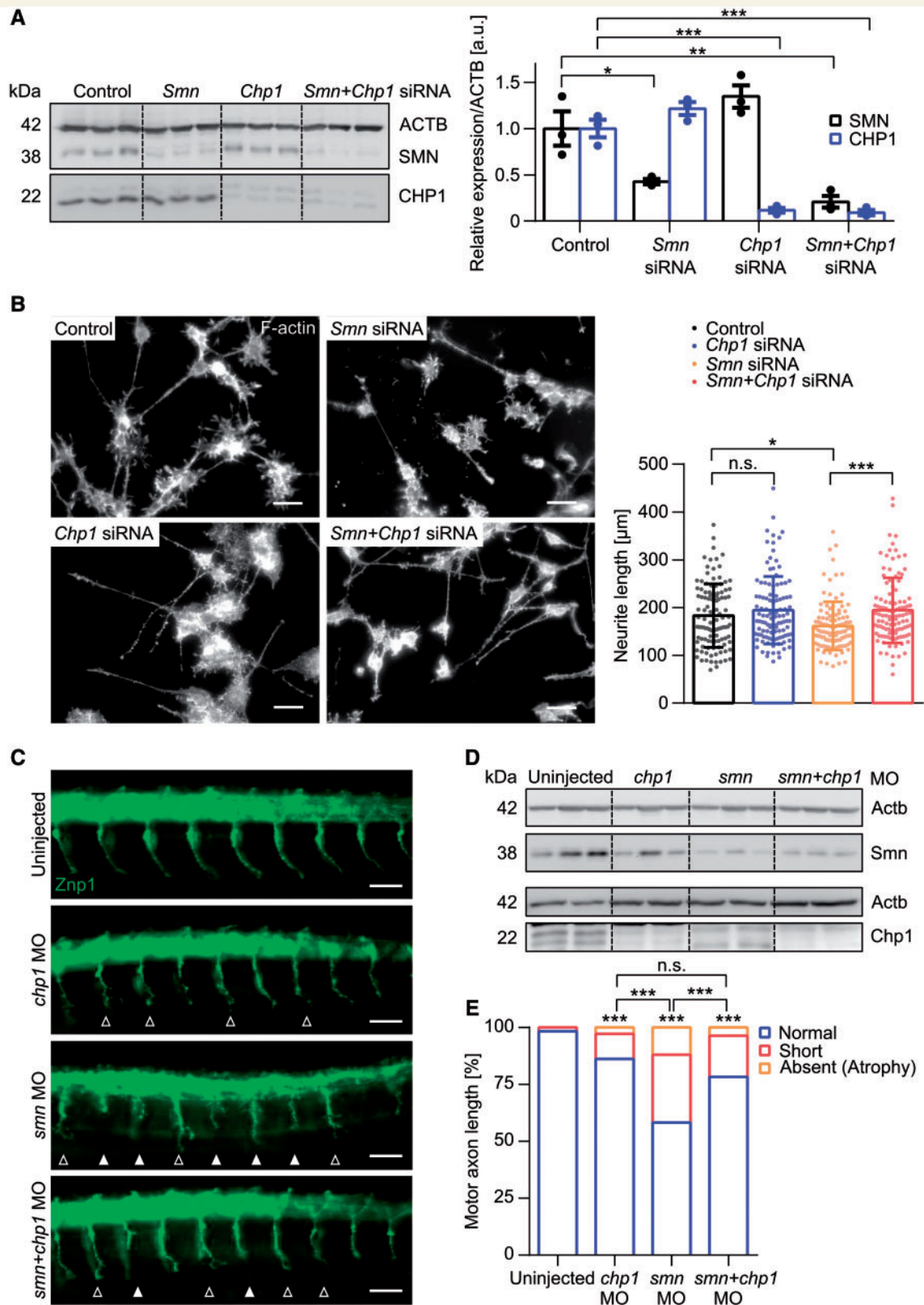
Figure 3 CHP1 downregulation improves neurite outgrowth in *Smn*-depleted NSC34 motor neuron-like cells and in zebrafish.
(**A**) Western blot analysis of siRNA-mediated knockdown of *Chp1* and *Smn* in NS34 cells. At 72 h post-transfection and retinoic acid-induced differentiation, CHP1 and SMN are significantly reduced (ACTB: loading control). *$P < 0.05$, **$P < 0.01$, ***$P < 0.001$, unpaired two-tailed Student's *t*-test. Error bars represent SEM. (**B**) Representative images and quantification of neurite length of NSC34 cells, transfected with the respective siRNA and differentiated with retinoic acid for 72 h. The reduced neurite length in *Smn*-depleted NSC34 cells was restored to control level by *Chp1* knockdown ($N = 3$, $n = 110$). F-actin was stained with phalloidin. Scale bar = 50 μm. *$P < 0.05$, ***$P < 0.001$, unpaired two-tailed

(continued)

reduced motor neuron area and reduced number of proprioceptive inputs per motor neuron compared to controls. Importantly, additional CHP1 reduction improved both motor neuron area and proprioceptive input number (Fig. 5B). Moreover, we found in transversus abdominis muscle increased NMJ size and restored NMJ maturity by additional CHP1 reduction in SMA-*Chp1*$^{vac/wt}$ + ASO mice compared to SMA + ASO mice alone (Fig. 5C). However, heterozygous *Chp1* mutation had no significant influence on mean muscle fibre size, but showed a clear trend towards a reduced number of small-sized muscle fibres ($<300 \mu m^2$) and an increased number of medium-sized muscle fibres ($300–500 \mu m^2$) in SMA-*Chp1*$^{vac/wt}$ + ASO versus SMA + ASO mice at postnatal Day 21 (Fig. 5D). In summary, these findings demonstrate that CHP1 reduction has a beneficial effect on well-characterized hallmarks of SMA, providing compelling evidence for CHP1 reduction to be a novel SMA protective modifier.

CHP1 downregulation rescues dynamin- and calcineurin-dependent impaired endocytosis in SMA

Since our data indicate that CHP1 is a modifier for SMA, we aimed to unveil the molecular mechanism behind the ameliorating effect. In recent studies, we showed that endocytosis is impaired and the Ca^{2+} influx is reduced in SMA. Interestingly, both modifiers, PLS3 overexpression and NCALD reduction, rescued decreased endocytosis, indicating that endocytosis is one of the most important affected pathways in SMA (Hosseinibarkooie *et al.*, 2016; Riessland *et al.*, 2017).

CHP1 is a Ca^{2+} binding protein involved in multiple processes, including membrane trafficking (Barroso *et al.*, 1996), microtubule dynamics (Andrade *et al.*, 2004), transcription (Lin *et al.*, 1999), pH homeostasis (Pang *et al.*, 2001; Liu *et al.*, 2013) and apoptosis (Kuwahara *et al.*, 2003). Most importantly, CHP1 interacts with calcineurin (CaN, PP2B), an important Ca^{2+}/calmodulin-dependent phosphatase and major regulator of essential proteins required for presynaptic endocytosis (Baumgartel and Mansuy, 2012). Overexpression of CHP1 in CCL39 fibroblasts leads to a 50% decrease of calcineurin phosphatase activity (Lin *et al.*, 1999); consequently, CHP1 is an endogenous calcineurin inhibitor.

Based on these findings, we hypothesized that CHP1 influences endocytosis via modulating calcineurin activity and thereby countering SMA pathology. To ascertain the impact of CHP1 reduction on endocytosis, we conducted knockdown studies followed by endocytosis assays. Since previous studies indicate that in SMA clathrin-independent bulk endocytosis as well as clathrin-dependent endocytosis are disturbed (Hosseinibarkooie *et al.*, 2016; Riessland *et al.*, 2017), we performed specific endocytosis assays for clathrin-independent macropinocytosis—formation of large endocytic vacuoles in unstimulated cells resembling bulk endocytosis in neurons—(FITC-dextran uptake) and clathrin-dependent receptor-mediated endocytosis (transferrin uptake) (Le Roy and Wrana, 2005). In neurons, bulk endocytosis can be specifically monitored by large fluorescent dextrans, which are too large to be accumulated in synaptic vesicles (Holt *et al.*, 2003; Clayton *et al.*, 2008). To detect large endocytic vacuoles formed by macropinocytosis, FITC-dextran (70 kDa) was considered as a suitable marker. In NSC34 cells, siRNA-mediated knockdown of *Smn* or *Chp1* or both was confirmed by western blotting (Supplementary Fig. 7A and D). Indeed, *Smn*-depleted NSC34 cells showed decreased FITC-dextran uptake, whereas *Chp1* knockdown resulted in an up to 3-fold increase of FITC-dextran endocytosis compared to control cells. Most interestingly, combined *Smn* and *Chp1* knockdown restored impaired endocytic FITC-dextran uptake compared to *Smn*-depleted cells (Fig. 6A and Supplementary Fig. 7C). In contrast, *Smn*- and *Chp1*-depleted cells showed no difference in clathrin-mediated transferrin endocytosis compared to control cells, respectively (Fig. 6B and Supplementary Fig. 7E).

To unveil the mechanism behind the increased macropinocytosis upon *Chp1* knockdown, we treated *Chp1*-depleted cells with inhibitors of major endocytic proteins. When treating cells with Dynasore—an inhibitor of dynamin, a GTPase required for membrane fission during endocytosis (Macia *et al.*, 2006)—we observed a marked reduction of endocytosis in control as well as in *Chp1*-depleted cells (Fig. 6C and Supplementary Fig. 7G), suggesting that the increased endocytosis in *Chp1*-depleted cells is dynamin-dependent. Since CHP1 was reported to regulate calcineurin, we investigated the effect of CHP1 during endocytosis when calcineurin is inhibited. Therefore, we treated cells with the calcineurin inhibitor

Figure 3 Continued

Student's *t*-test and Holm correction for multiple comparison. Error bars represent SD. (**C**) Representative images of motor axons posterior to the yolk globule of 34 hpf zebrafish embryos injected with the respective morpholinos (MOs) and labelled with α-Znp1 antibody. Zebrafish embryos were injected at the 1–4 cell stage with 2 ng *chp1*, *smn* morpholino, or both and further analysed 34 hpf. Motor axons of *smn*-depleted fish show severe truncations (absent or shortened axons) and branching phenotypes, which are ameliorated upon co-injection with *chp1* morpholino. Scale bar = 50 μm. Solid arrowheads indicate truncated and absent axons, open arrowheads indicate terminal branching. (**D**) Western blotting demonstrates the morpholino-mediated knockdown of *smn* and *chp1*, respectively. Actb = loading control. (**E**) Quantitative analysis of caudal primary motor neurons shows that co-injection of *smn* and *chp1* morpholinos ameliorates the frequencies of reduced motor axon length (absent or shortened axons) of *smn* morphants ($n > 150$ analysed motor axons). ***$P < 0.001$, Chi-square test. n.s. = not significant.
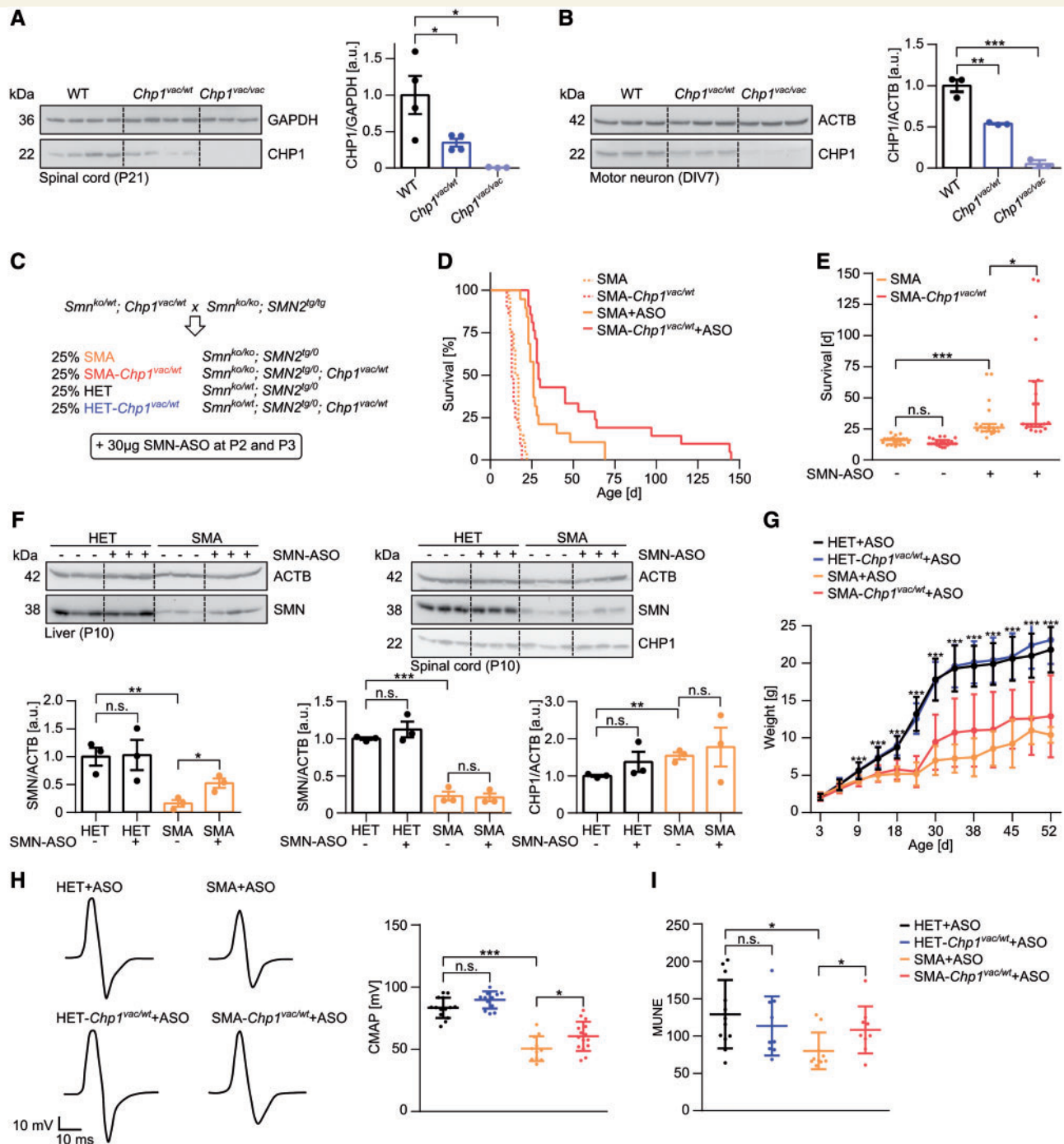
Figure 4 CHP1 reduction additionally improves the phenotype of a low-dose SMN-ASO-injected severe SMA mouse model.
(**A**) Western blot analysis of CHP1 level in spinal cord of vacillator mice at postnatal Day (P) 21. CHP1 is reduced to <50% in spinal cord of heterozygous ($Chp1^{vac/wt}$) and almost absent in homozygous ($Chp1^{vac/vac}$) mice ($N = 3–4$). ACTB = loading control. *$P < 0.05$, unpaired two-tailed Student's t-test. Error bars represent SEM. (**B**) Western blot analysis of CHP1 level in motor neurons derived from wild-type, $Chp1^{vac/wt}$ and $Chp1^{vac/vac}$ embryonic Day 12.5–13.5 embryos at in vitro Day 7. CHP1 is reduced to 50% in primary motor neurons from $Chp1^{vac/wt}$ and almost absent in $Chp1^{vac/vac}$ embryos ($N = 3$). ACTB = loading control. **$P < 0.01$, ***$P < 0.001$, unpaired two-tailed Student's t-test. Error bars represent SEM. (**C**) Breeding scheme to produce SMA, SMA-$Chp1^{vac/wt}$, HET and HET-$Chp1^{vac/wt}$ mice in a congenic C57BL/6 N background. All offspring were subcutaneously injected with 30 μg SMN-ASO at postnatal Days 2 and 3. (**D**) Kaplan-Meier curves of uninjected and SMN-ASO-injected mice show a significant prolongation of survival in SMA-$Chp1^{vac/wt}$ + ASO versus SMA + ASO mice. No difference in lifespan was present in SMA-$Chp1^{vac/wt}$ compared to non-treated SMA mice ($N = 19–21$). (**E**) Median survival and interquartile range of SMA and SMA-$Chp1^{vac/wt}$ mice uninjected and low-dose SMN-ASO-injected. Median survival: SMA = 16 days, SMA-$Chp1^{vac/wt}$ = 13 days, SMA + ASO = 26 days, SMA-$Chp1^{vac/wt}$ + ASO = 31 days. Mean survival ± SD: SMA = 15.75 ± 3 days, SMA-$Chp1^{vac/wt}$ = 14.3 ± 3 days, SMA + ASO = 31.15 ± 15 days, SMA-$Chp1^{vac/wt}$ + ASO = 51.95 ± 39. *$P < 0.05$, ***$P < 0.001$, log-rank (Mantel-Cox) test and exact Wilcoxon-Rank test. (**F**) Western blot

(continued)

cyclosporin A (Liu *et al.*, 1991). Indeed, we found a reduced endocytosis in *Chp1*-depleted cells upon cyclosporin A treatment (Fig. 6D and Supplementary Fig. 7I), suggesting that the elevated endocytosis upon CHP1 knockdown is calcineurin activity-dependent. *Chp1* knockdown was not affected by treatment with Dynasore and cyclosporin A (Supplementary Fig. 7F and H). In summary, we show that CHP1 downregulation dramatically enhances macropinocytosis but not clathrin-mediated endocytosis and rescues impaired endocytosis in SMA. Furthermore, these processes are dependent on dynamin and calcineurin activity.

CHP1 reduction increases calcineurin activity counteracting dynamin 1 hyperphosphorylation in SMA

To assess whether CHP1 reduction increases calcineurin activity and thereby induces endocytosis, we performed a specific cellular calcineurin phosphatase activity assay to detect the phosphorylation of the RII phosphopeptide—the most specific substrate of calcineurin activity (Roberts *et al.*, 2008). Importantly, *Chp1* depletion increased free phosphate, indicating an elevated calcineurin phosphatase activity (Fig. 7A). In line with this, we detected decreased levels of phospho-dynamin 1 (pDNM1) in *Chp1*-depleted cells (Fig. 7B) as well as in hippocampal neurons from vacillator mice (Supplementary Fig. 8B), proving that CHP1 downregulation results in increased calcineurin phosphatase activity. Notably, the calcineurin level itself did not change upon *Chp1* knockdown (Supplementary Fig. 8A). Previous studies have reported a reduced Ca^{2+} influx (Riessland *et al.*, 2017) as well as cyclin-dependent kinase 5 (CDK5) hyperactivity in SMA (Miller *et al.*, 2015). CDK5 phosphorylates dynamin 1 (DNM1) (Tan *et al.*, 2003). Therefore, we assessed calcineurin activity as well as DNM1 phosphorylation in SMA. Indeed, *Smn*-depleted NSC34 cells showed diminished calcineurin activity (Fig. 7C). Moreover, *Smn*-depleted NSC34 cells (Fig. 7D) and motor neurons from SMA mice (Fig. 7E) showed a robust increase of pDNM1. In congruence with our observations in NSC34 cells (Fig. 7A), CHP1 reduction in HET-*Chp1*$^{vac/wt}$ motor neurons resulted in decreased pDNM1 (Fig. 7E). Remarkably,

downregulation of CHP1 reduced DNM1 hyperphosphorylation in SMA motor neurons (Fig. 7E). Collectively, we show DNM1 is hyperphosphorylated in SMA motor neurons, which could explain the reduced endocytosis in SMA. Furthermore, we demonstrate that CHP1 reduction increases calcineurin activity, which reduces DNM1 hyperphosphorylation in SMA motor neurons.

Discussion

In summary, our main results demonstrate: (i) CHP1 directly interacts with PLS3, a strong protective SMA modifier; (ii) CHP1 is ubiquitously present, but particularly abundant in neuronal tissues and at SMA relevant sites, including motor neuron soma and growth cones and presynaptic NMJ sites; (iii) CHP1 level is elevated in spinal cord and brain of SMA mice; (iv) *Chp1* depletion rescues reduced axonal outgrowth in various SMA models, including *Smn*-deficient NSC34 cells, zebrafish *smn* morphants and mouse primary motor neurons; (v) CHP1 reduction extends the lifespan and improves weight progression and electrophysiological defects of a low-dose SMN-ASO-treated SMA mouse model; (vi) CHP1 downregulation improves major SMA hallmarks in mice such as motor neuron soma area, proprioceptive input number, NMJ size and maturity, and muscle fibre size; (vii) *Chp1* knockdown rescues impaired macropinocytosis in *Smn*-deficient NSC34 cells; and (viii) in SMA, DNM1 is hyperphosphorylated; CHP1 depletion facilitates calcineurin phosphatase activity, which not only reduces DNM1 hyperphosphorylation but also counteracts impaired endocytosis in SMA.

Therapy studies of SMA1 individuals treated intrathecally with SPINRAZA™ (splice correction of *SMN2*) or intravenously with SMN-AAV9 (gene-replacement therapy) show impressive improvements in motoric abilities and survival (Finkel *et al.*, 2016, 2017; Mendell *et al.*, 2017). Upon successful clinical trials, SPINRAZA™ has recently been FDA- and EMA-approved for SMA therapy. Although SMN-dependent therapy markedly improves symptoms and increases survival, for SMA1 individuals, carrying only two *SMN2* copies (Finkel *et al.*, 2016, 2017), this approach may be insufficient and not curative.

Figure 4 Continued
analysis of liver and spinal cord lysates from uninjected and SMN-ASO-injected HET and SMA mice at postnatal Day 10. SMN levels were increased in liver, but not in spinal cord of SMA mice after SMN-ASO injection. SMN-ASO injection did not significantly change CHP1 levels in spinal cord compared to uninjected animals. ACTB = loading control. *$P < 0.05$, **$P < 0.01$, ***$P < 0.001$, unpaired two-tailed Student's *t*-test. Error bars represent SEM. (**G**) Weight progression of SMN-ASO-injected SMA and SMA-*Chp1*$^{vac/wt}$ mice in comparison to SMN-ASO-injected HET and HET-*Chp1*$^{vac/wt}$ mice. No significant difference but a trend of increased weight progression was observed between SMA + ASO and SMA-*Chp1*$^{vac/wt}$ + ASO mice From Day 9 on a significant difference between SMA + ASO and HET + ASO mice was observed ($N = 20$–30). *SMA tested against HET mice, ***$P < 0.001$, unpaired two-tailed Student's *t*-test. Error bars represent SD. (**H**) Sciatic CMAP response in SMA + ASO mice is markedly reduced as compared to HET + ASO mice, but significantly ameliorated by CHP1 reduction. Representative sciatic CMAP responses and quantification of SMN-ASO-injected mice at postnatal Day 21. The peak-to-peak amplitude was quantified ($N = 11$–15). *$P < 0.05$, ***$P < 0.001$, unpaired two-tailed Student's *t*-test and Holm correction for multiple comparison. Error bars represent SD. (**I**) MUNE is markedly reduced in SMA + ASO versus HET + ASO mice at postnatal Day 21. CHP1 reduction significantly improves MUNE in SMA-*Chp1*$^{vac/wt}$ mice compared to SMA + ASO mice ($N = 9$–12). *$P < 0.05$, unpaired two-tailed Student's *t*-test and Holm correction for multiple comparison. Error bars represent SD.
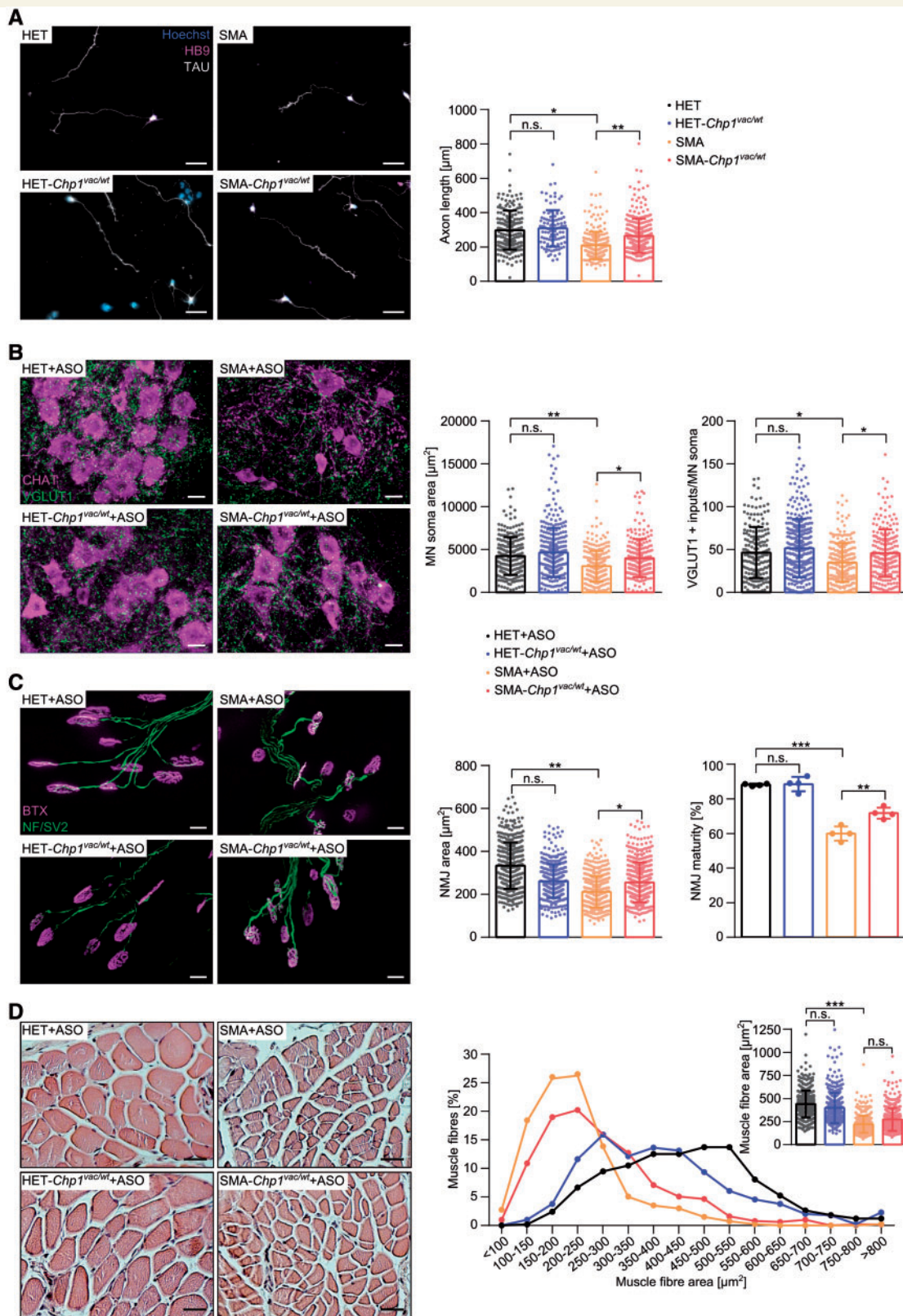
Figure 5 **Heterozygous *Chp1* mutation improves axonal outgrowth, proprioceptive input number, and NMJ size and maturity in low-dose SMN-ASO-injected severe SMA mice.** (**A**) Representative merged images and quantification of motor axon length of motor neurons isolated from E12.5-13.5 embryos at 5 DIV. CHP1 reduction (*Chp1*$^{vac/wt}$) alone has no effect on axonal outgrowth. In contrast, motor neurons derived from SMA mice show shorter motor axons, which were restored to HET levels by CHP1 reduction (SMA-*Chp1*$^{vac/wt}$). Motor neurons were stained with TAU (white, for axon), HB9 (magenta, for motor neuron) and Hoechst (blue, for nuclei). Scale bar = 50 μm.

(continued)

Thus, there is a need to identify additional pharmacological interventions to further improve their disease course. Therefore, a combinatorial treatment targeting SMN-dependent and SMN-independent pathways might be more promising (Wirth *et al.*, 2015). Importantly, PLS3 overexpression and NCALD reduction have been identified as the first SMN-independent modifiers of SMA (Oprea *et al.*, 2008; Riessland *et al.*, 2017). In recent studies, not only the stable overexpression of PLS3 but also the AAV9-mediated delivery of PLS3 have been shown to extend the lifespan of low-dose SMN-ASO-injected severe SMA mice (Hosseinibarkooie *et al.*, 2016; Kaifer *et al.*, 2017). These studies highlight the potential utility of combinatorial therapeutics in SMA that target both SMN-dependent and SMN-independent pathways.

To unveil the molecular mechanism behind the rescuing effect of PLS3 and to find new disease modifiers, which could be used as therapeutic targets, we screened for novel PLS3-interacting partners. Hereby, we identified CHP1 as a promising candidate that directly interacts with PLS3. Remarkably, the CHP1 level was increased in severely-affected SMA mice. Consequently, we postulated that CHP1 reduction might be beneficial to counteract the SMA phenotype. Indeed, analysis of low-dose SMN-ASO-injected severely-affected SMA mice presenting reduced CHP1 levels showed a significantly extended lifespan and improvement of all well-characterized SMA hallmarks compared to low-dose SMN-ASO-injected SMA mice alone.

Since CHP1 was reported to be a calcineurin inhibitor (Lin *et al.*, 1999), increased CHP1 levels most likely results in decreased calcineurin activity in SMA. Calcineurin is a Ca^{2+}-calmodulin-dependent phosphatase universally involved in vesicle endocytosis in neuronal and non-neuronal secretory cells (Wu *et al.*, 2014). In detail, during elevated neuronal activity calcineurin is activated by Ca^{2+} influx and dephosphorylates various dephosphins, including DNM1 (Cousin and Robinson, 2001). DNM1 dephosphorylation stimulates a specific DNM1-syndapin 1 interaction, which triggers activity-dependent bulk endocytosis to massively increase synaptic vesicle endocytosis (Clayton *et al.*, 2009). Finally, after the scission of bulk endosomes, DNM1 is rephosphorylated by CDK5 (Evans and Cousin, 2007) and glycogen synthase kinase 3 (GSK3) (Smillie and Cousin, 2012). Among all types of endocytosis, bulk endocytosis is of particular importance in neurons as it is the dominant mode during intense neuronal activity (Clayton *et al.*, 2008). Interestingly, increased CDK5 activity was reported in both SMA mice and human SMA induced pluripotent stem cell-derived motor neurons (Miller *et al.*, 2015). Consequently, the aberrant endocytosis in SMA might be caused not only by decreased Ca^{2+} influx and disturbed F-actin levels (Hosseinibarkooie *et al.*, 2016; Riessland *et al.*, 2017), but also by increased CDK5 activity as well as reduced calcineurin activity caused either by increased CHP1 expression and/or by reduced Ca^{2+} influx failing to completely activate calcineurin. Importantly, we not only show for the first time that calcineurin activity is reduced in *Smn*-depleted cells but also that CHP1 reduction increases endocytosis due to an increased calcineurin activity and thereby promotes DNM1 dephosphorylation, which counteracts DNM1 hyperphosphorylation in SMA motor neurons. These findings indicate that CHP1 reduction improves macropinocytosis not only in NSC34 cells by increasing calcineurin activity, but also neuronal bulk endocytosis in primary motor neurons. In line with this, we demonstrate that CHP1 downregulation rescues reduced axonal outgrowth in various SMA models. Interestingly, DNM1 dephosphorylation by calcineurin was previously linked to neurotrophin receptor endocytosis, thus promoting axonal growth (Bodmer *et al.*, 2011). The latter strongly suggests that upon CHP1 reduction, increased calcineurin-dependent DNM1 dephosphorylation stimulates growth factor endocytosis and thereby axonal growth. Of note, motor neurons are particularly vulnerable to defects in endocytosis because of their high firing rate and large synapses. Since, SMA motor neurons are hyperexcitable (Gogliotti *et al.*, 2012), they might additionally have a higher demand of

Figure 5 Continued

Quantification of the longest axon with ZEN software (Zeiss) ($N = 3–7$, $n = 20–50$ motor neurons/embryo). *$P < 0.05$, **$P < 0.01$, unpaired two-tailed Student's *t*-test and Holm correction for multiple comparison of mean per embryo. Error bars represent SD. (**B**) Representative merged images and quantification of motor neuron soma surface area and proprioceptive input number (VGLUT1, green) per motor neuron soma (CHAT, magenta) in lumbar regions of the spinal cord of low-dose SMN-ASO-injected mice at postnatal Day 21. Scale bar = 20 μm. CHP1 reduction ameliorates decreased motor neuron soma and number of proprioceptive inputs per motor neuron soma in SMA mice. Mean input number within 5 μm of motor neuron soma was analysed with ImageJ ($N = 3–4$, $n = 40–60$ motor neurons/mouse). *$P < 0.05$, **$P < 0.01$, unpaired two-tailed Student's *t*-test and Holm correction for multiple comparison of mean per mouse. Error bars represent SD. (**C**) Representative images and quantification of NMJ area and maturity in transversus abdominis muscle of SMN-ASO-injected mice at postnatal Day 21, stained with NF-M and SV2 (green) and BTX (magenta). Scale bar = 20 μm. CHP1 reduction improved NMJ size and the number of mature NMJs in SMA mice. NMJ area was analysed with ImageJ ($N = 4$, $n = 100$ NMJs/mouse). *$P < 0.05$, **$P < 0.01$, ***$P < 0.001$, unpaired two-tailed Student's *t*-test and Holm correction for multiple comparison of mean per mouse. Error bars represent SD. (**D**) Representative pictures of haematoxylin and eosin staining and quantification of muscle fibre size of tibialis anterior (TA) muscle from low-dose SMN-ASO-injected mice at postnatal Day 21. Scale bar = 250 μm. Muscle fibre size was measured with ZEN software ($N = 4–5$, $n = 100$ fibres/mouse). For visualization, muscle fibres were grouped according to area intervals of 50 μm^2. ***$P < 0.001$, unpaired two-tailed Student's *t*-test and Holm correction for multiple comparison of mean per mouse. Error bars represent SD. n.s. = not significant.
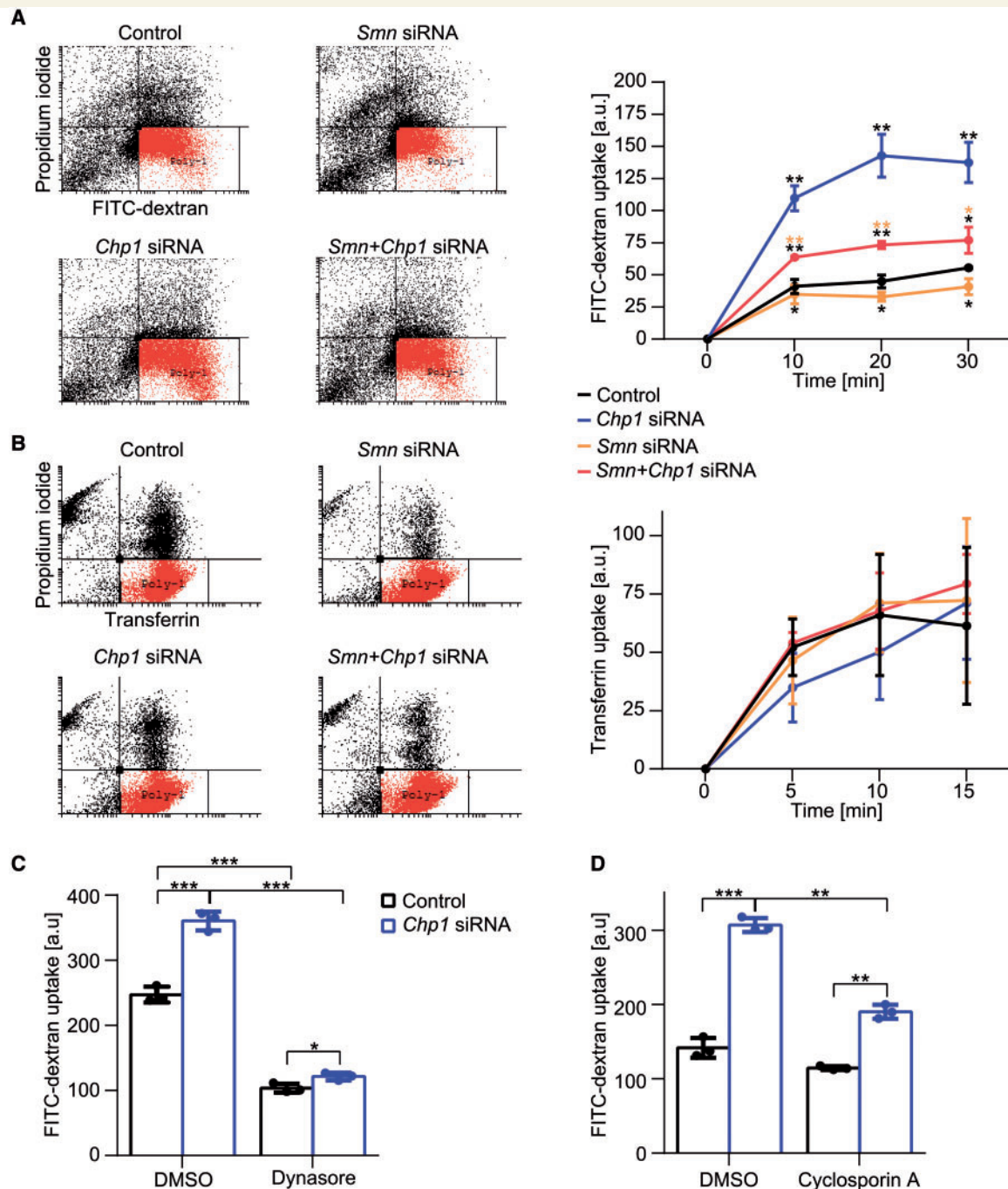
Figure 6 CHP1 reduction rescues impaired macropinocytosis in *Smn*-depleted motor neuron-like cells. (**A**) Representative FACS dot plots (20 min) and quantification of the Poly-1 cell population of FITC-dextran (70 kDa) uptake, measuring macropinocytosis, in NSC34 cells. Knockdown of *Chp1* highly improves FITC-dextran uptake and restores impaired FITC-dextran uptake in *Smn*-deficient cells. NSC34 cells were incubated for 10, 20 and 30 min with FITC-dextran. FITC-dextran uptake of gated Poly-1 cell population was measured by FACS ($N = 3$, $n = 20\,000$ cells). Dead cells were detected by propidium iodide. Black asterisk indicates tested against control; orange asterisk indicates tested against *Smn*-depleted cells. $*P < 0.05$, $**P < 0.01$, unpaired two-tailed Student's *t*-test. Error bars represent SEM. (**B**) Representative FACS dot plots (20 min) and quantification of the Poly-1 cell population of transferrin uptake, measuring clathrin-mediated endocytosis, in NSC34 cells. Clathrin-mediated endocytosis is not changed upon *Smn* knockdown. NSC34 cells depleted for CHP1 and SMN were incubated for 5, 10 and 15 min with transferrin and measured by FACS ($N = 3$, $n = 20\,000$ cells). Dead cells were detected by propidium iodide. Error bars represent SEM. (**C**) *Chp1* knockdown effect in FITC-dextran uptake is dynamin-dependent. Inhibition of dynamin by Dynasore treatment, abolished the enhanced FITC-dextran endocytic uptake by *Chp1* knockdown. Control cells were treated with DMSO. FITC-dextran uptake was measured by FACS ($N = 3$, $n = 20\,000$ cells). $*P < 0.05$, $***P < 0.001$, unpaired two-tailed Student's *t*-test. Error bars represent SEM. (**D**) Inhibition of calcineurin phosphatase activity with cyclosporin A (CsA) reduces FITC-dextran uptake upon *Chp1* knockdown. Control cells were treated with DMSO. Uptake was measured by FACS ($N = 3$, $n = 20\,000$ cells). $**P < 0.01$, $***P < 0.001$, unpaired two-tailed Student's *t*-test. Error bars represent SEM.
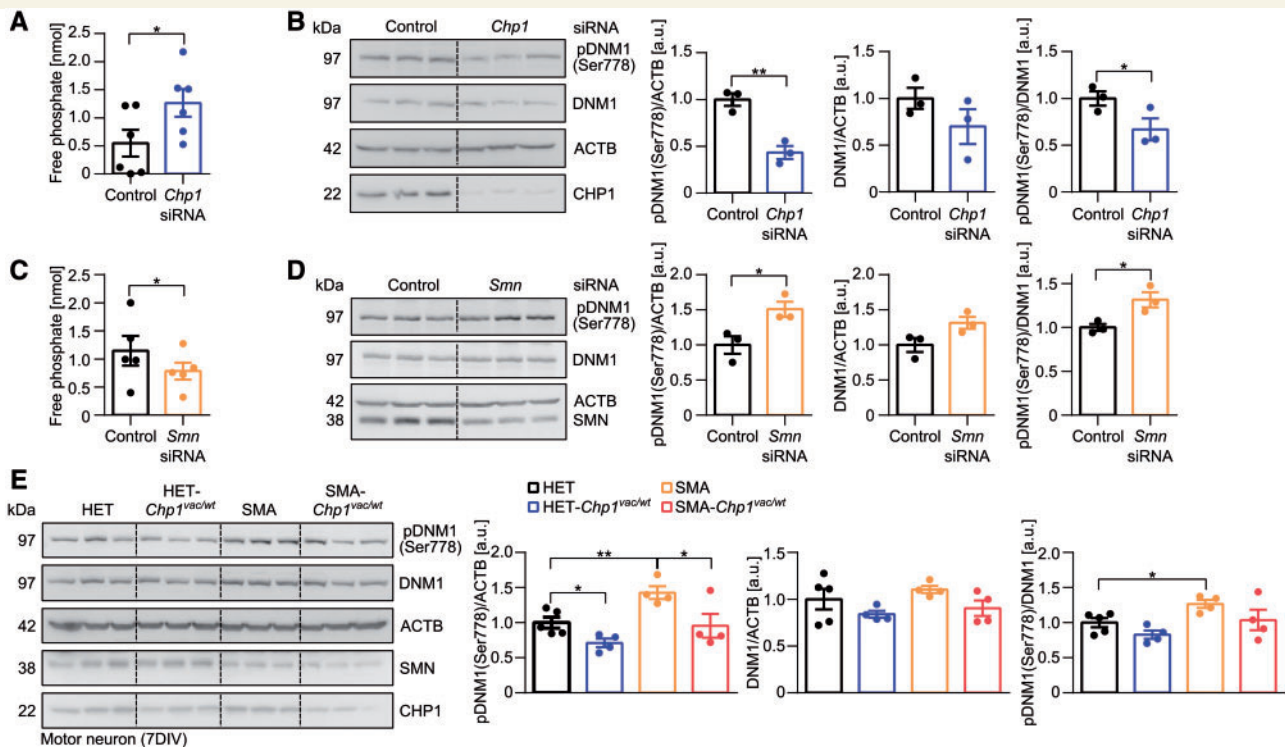
Figure 7 ***Chp1* knockdown increases calcineurin phosphatase activity and counteracts DNM1 hyperphosphorylation in SMA.**
(**A**) *Chp1* knockdown increases calcineurin phosphatase activity. Cellular calcineurin phosphatase activity was investigated in transfected NSC34 cells by measuring the phosphorylation of the RII phosphopeptide, a specific substrate of calcineurin ($N = 6$). *$P < 0.05$, paired, two-tailed Student's *t*-test. Error bars represent SEM. (**B**) Western blot analysis shows decreased phosphorylated dynamin 1 (pDNM1) in *Chp1*-depleted NSC34 cells. Phosphorylation of DNM1 was investigated by specific antibodies recognizing the Ser-778 phosphorylation site. ACTB = loading control. **$P < 0.01$, unpaired two-tailed Student's *t*-test. Error bars represent SEM. (**C**) *Smn* knockdown diminishes calcineurin phosphatase activity in NSC34 cells ($N = 5$). *$P < 0.05$, paired, two-tailed Student's *t*-test. Error bars represent SEM. (**D**) Western blot analysis indicates increased pDNM1 in *Smn*-depleted NSC34 cells. ACTB = loading control. *$P < 0.05$, unpaired two-tailed Student's *t*-test. Error bars represent SEM. (**E**) Representative western blot and quantification shows increased pDNM1 in SMA motor neurons, which was restored to HET levels in SMA-*Chp1*$^{vac/wt}$, and furthermore decreased in HET-*Chp1*$^{vac/wt}$ motor neurons at *in vitro* Day 7. Total DNM1 level was not changed ($N = 4$–5). ACTB = loading control. *$P < 0.05$, **$P < 0.01$, unpaired two-tailed Student's *t*-test. Error bars represent SEM.

endocytosis to recycle synaptic vesicles and retrieve membrane. Therefore, disturbances in presynaptic vesicle recycling severely reduce neurotransmission caused by decreased replenishment of the synaptic vesicle pool, reduced clearance of release sites, disturbed presynaptic integrity and reduced membrane retrieval. Previous studies showed impaired neurotransmission and decreased synaptic vesicle number in SMA (Kong *et al.*, 2009; Torres-Benito *et al.*, 2012). More recently, defects in endocytosis were shown to contribute to SMA pathology at the NMJ level (Dimitriadi *et al.*, 2016; Hosseinibarkooie *et al.*, 2016; Riessland *et al.*, 2017). Taken together, our study further emphasizes the importance of the endocytic pathway as a key-affected pathway in SMA. We suggest that CHP1 downregulation ameliorates the SMA phenotype by improving the impaired bulk endocytosis by inducing calcineurin activity and DNM1 dephosphorylation (Fig. 8).

Interestingly, compared to CHP1 reduction, NCALD knockdown has a positive effect only in a mild but not in an intermediate low-dose SMN-ASO-induced SMA mouse model (Riessland *et al.*, 2017). Thus, CHP1 reduction appears to be a stronger protective modifier. This difference might be due to the ubiquitous presence of CHP1, which guarantees a systemic effect, while NCALD is mainly restricted to neuronal tissues. Additionally, NCALD suppression improves clathrin-mediated endocytosis (Riessland *et al.*, 2017), whereas CHP1 suppression improves bulk endocytosis, which is particularly required in neurons with frequent firing (Clayton *et al.*, 2008). In contrast, PLS3 overexpression showed the highest effect in the SMN-ASO-injected severe SMA mouse model so far. PLS3 also improves bulk endocytosis by increasing F-actin levels but further counteracts F-actin-dependent processes impaired in SMA, both at motor neuron and NMJ level (Ackermann *et al.*, 2013; Hosseinibarkooie *et al.*, 2016). Importantly, overexpression of a certain gene is more difficult to achieve than knockdown, a combinatorial therapy using CHP1- and SMN-ASOs could be highly promising for future therapy in SMA, especially in SMA1-affected individuals.
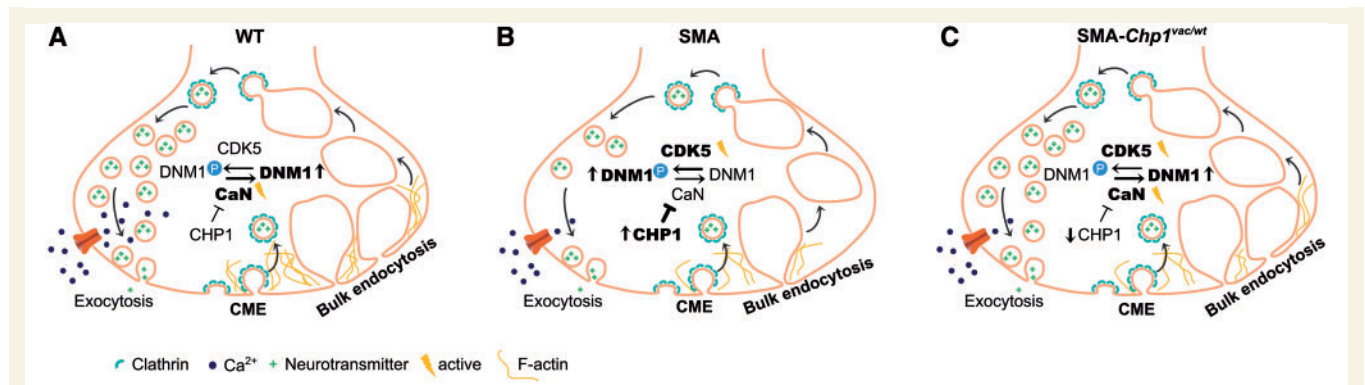
Figure 8 CHP1 downregulation improves endocytosis by increasing calcineurin phosphatase activity. (**A**) In wild-type (WT), upon stimulation Ca²⁺ influx activates calcineurin (CaN) activity leading to DNM1 dephosphorylation, thereby allowing DNM1 and syndapin1 interaction and triggering bulk endocytosis. Cyclin dependent kinase 5 (CDK5) rephosphorylates DNM1 and stops bulk endocytosis. (**B**) In SMA, decreased F-actin levels impair endocytosis (Hosseinibarkooie et al., 2016). Elevated CHP1 levels and decreased Ca²⁺ influx, lead to decreased CaN activity. CDK5 activity is increased in SMA (Miller et al., 2015). Decreased CaN activity as well as increased CDK5 activity cause dynamin 1 (DNM1) hyperphosphorylation, which blocks its interaction with syndapin 1; consequently, bulk endocytosis is inhibited in SMA. (**C**) CHP1 downregulation in SMA rescues impaired endocytosis. CHP1 reduction increases calcineurin activity, which leads to increased DNM1 dephosphorylation thereby, allowing DNM1-syndapin 1 interaction, which triggers bulk endocytosis. Hereby, increased calcineurin activity compensates for both reduced Ca²⁺ influx and increased CDK5 activity in SMA. CME = clathrin-mediated endocytosis.

Since endocytosis defects and Ca²⁺ misregulation have also been reported in Parkinson's disease, amyotrophic lateral sclerosis, and hereditary spastic paraplegias (Schreij et al., 2016), CHP1 downregulation might be beneficial for the treatment of other neurodegenerative diseases. Strikingly, in multiple sclerosis patients, interferon-β treatment—a first line therapy for multiple sclerosis—was found to downregulate *CHP1* mRNA expression (Srinivasan et al., 2017), suggesting a beneficial effect of CHP1 reduction in multiple sclerosis too. Moreover, calcineurin-related pathways like NGF signalling are involved in neurodegeneration of Down syndrome (Cooper et al., 2001). Furthermore, reduction of calcineurin activity has been implicated in Alzheimer's disease (Ladner et al., 1996), whereas overexpression of a regulator of calcineurin 1—an endogenous calcineurin inhibitor—has been associated with Alzheimer's disease and Down syndrome (Ermak et al., 2001). Therefore, induction of calcineurin activity by downregulation of its endogenous inhibitor CHP1 might be used as a cross-disease therapy targeting a common pathogenic pathway.

Supplementary material

Supplementary material is available at *Brain* online.

References

Ackermann B, Krober S, Torres-Benito L, Borgmann A, Peters M, Hosseini Barkooie SM, et al. Plastin 3 ameliorates spinal muscular atrophy via delayed axon pruning and improves neuromuscular junction functionality. Hum Mol Genet 2013; 22: 1328–47.

Akten B, Kye MJ, Hao le T, Wertz MH, Singh S, Nie D, et al. Interaction of survival of motor neuron (SMN) and HuD proteins with mRNA cpg15 rescues motor neuron axonal deficits. Proc Natl Acad Sci USA 2011; 108: 10337–42.

Andrade J, Zhao H, Titus B, Timm Pearce S, Barroso M. The EF-hand Ca2 + -binding protein p22 plays a role in microtubule and

endoplasmic reticulum organization and dynamics with distinct Ca2 + -binding requirements. Mol Biol Cell 2004; 15: 481–96.

Arnold WD, Sheth KA, Wier CG, Kissel JT, Burghes AH, Kolb SJ. Electrophysiological Motor Unit Number Estimation (MUNE) Measuring Compound Muscle Action Potential (CMAP) in mouse hindlimb muscles. J Vis Exp 2015; 103: 52899.

Barroso MR, Bernd KK, DeWitt ND, Chang A, Mills K, Sztul ES. A novel Ca2 + -binding protein, p22, is required for constitutive membrane traffic. J Biol Chem 1996; 271: 10183–7.

Baumgartel K, Mansuy IM. Neural functions of calcineurin in synaptic plasticity and memory. Learn Mem 2012; 19: 375–84.

Bodmer D, Ascano M, Kuruvilla R. Isoform-specific dephosphorylation of dynamin1 by calcineurin couples neurotrophin receptor endocytosis to axonal growth. Neuron 2011; 70: 1085–99.

Bogdanik LP, Osborne MA, Davis C, Martin WP, Austin A, Rigo F, et al. Systemic, postsymptomatic antisense oligonucleotide rescues motor unit maturation delay in a new mouse model for type II/III spinal muscular atrophy. Proc Natl Acad Sci USA 2015; 112: E5863–72.

Bolte S, Cordelieres FP. A guided tour into subcellular colocalization analysis in light microscopy. J Microsc 2006; 224(Pt. 3): 213–32.

Cartegni L, Hastings ML, Calarco JA, de Stanchina E, Krainer AR. Determinants of exon 7 splicing in the spinal muscular atrophy genes, SMN1 and SMN2. Am J Hum Genet 2006; 78: 63–77.

Cartegni L, Krainer AR. Disruption of an SF2/ASF-dependent exonic splicing enhancer in SMN2 causes spinal muscular atrophy in the absence of SMN1. Nat Genet 2002; 30: 377–84.

Clayton EL, Anggono V, Smillie KJ, Chau N, Robinson PJ, Cousin MA. The phospho-dependent dynamin-syndapin interaction triggers activity-dependent bulk endocytosis of synaptic vesicles. J Neurosci 2009; 29: 7706–17.

Clayton EL, Evans GJ, Cousin MA. Bulk synaptic vesicle endocytosis is rapidly triggered during strong stimulation. J Neurosci 2008; 28: 6627–32.

Cooper JD, Salehi A, Delcroix JD, Howe CL, Belichenko PV, Chua-Couzens J, et al. Failed retrograde transport of NGF in a mouse model of Down's syndrome: reversal of cholinergic neurodegenerative phenotypes following NGF infusion. Proc Natl Acad Sci USA 2001; 98: 10439–44.

Cousin MA, Robinson PJ. The dephosphins: dephosphorylation by calcineurin triggers synaptic vesicle endocytosis. Trends Neurosci 2001; 24: 659–65.

Dimitriadi M, Derdowski A, Kalloo G, Maginnis MS, O'Hern P, Bliska B, et al. Decreased function of survival motor neuron protein impairs endocytic pathways. Proc Natl Acad Sci USA 2016; 113: E4377–86.

Dimitriadi M, Sleigh JN, Walker A, Chang HC, Sen A, Kalloo G, et al. Conserved genes act as modifiers of invertebrate SMN loss of function defects. PLoS Genet 2010; 6: e1001172.

El-Khodor BF, Edgar N, Chen A, Winberg ML, Joyce C, Brunner D, et al. Identification of a battery of tests for drug candidate evaluation in the SMNDelta7 neonate model of spinal muscular atrophy. Exp Neurol 2008; 212: 29–43.

Ermak G, Morgan TE, Davies KJ. Chronic overexpression of the calcineurin inhibitory gene DSCR1 (Adapt78) is associated with Alzheimer's disease. J Biol Chem 2001; 276: 38787–94.

Evans GJ, Cousin MA. Activity-dependent control of slow synaptic vesicle endocytosis by cyclin-dependent kinase 5. J Neurosci 2007; 27: 401–11.

Feldkotter M, Schwarzer V, Wirth R, Wienker TF, Wirth B. Quantitative analyses of SMN1 and SMN2 based on real-time lightCycler PCR: fast and highly reliable carrier testing and prediction of severity of spinal muscular atrophy. Am J Hum Genet 2002; 70: 358–68.

Finkel RS, Chiriboga CA, Vajsar J, Day JW, Montes J, De Vivo DC, et al. Treatment of infantile-onset spinal muscular atrophy with nusinersen: a phase 2, open-label, dose-escalation study. Lancet 2016; 388: 3017–26.

Finkel RS, Mercuri E, Darras BT, Connolly AM, Kuntz NL, Kirschner J, et al. Nusinersen versus Sham control in infantile-onset spinal muscular atrophy. N Engl J Med 2017; 377: 1723–32.

Flanagan-Steet H, Fox MA, Meyer D, Sanes JR. Neuromuscular synapses can form *in vivo* by incorporation of initially aneural postsynaptic specializations. Development 2005; 132: 4471–81.

Gogliotti RG, Quinlan KA, Barlow CB, Heier CR, Heckman CJ, Didonato CJ. Motor neuron rescue in spinal muscular atrophy mice demonstrates that sensory-motor defects are a consequence, not a cause, of motor neuron dysfunction. J Neurosci 2012; 32: 3818–29.

Hamilton G, Gillingwater TH. Spinal muscular atrophy: going beyond the motor neuron. Trends Mol Med 2013; 19: 40–50.

Hao le T, Wolman M, Granato M, Beattie CE. Survival motor neuron affects plastin 3 protein levels leading to motor defects. J Neurosci 2012; 32: 5074–84.

Holt M, Cooke A, Wu MM, Lagnado L. Bulk membrane retrieval in the synaptic terminal of retinal bipolar cells. J Neurosci 2003; 23: 1329–39.

Hosseinibarkooie S, Peters M, Torres-Benito L, Rastetter RH, Hupperich K, Hoffmann A, et al. The power of human protective modifiers: PLS3 and CORO1C unravel impaired endocytosis in spinal muscular atrophy and rescue SMA phenotype. Am J Hum Genet 2016; 99: 647–65.

Hsieh-Li HM, Chang JG, Jong YJ, Wu MH, Wang NM, Tsai CH, et al. A mouse model for spinal muscular atrophy. Nat Genet 2000; 24: 66–70.

Hua Y, Sahashi K, Rigo F, Hung G, Horev G, Bennett CF, et al. Peripheral SMN restoration is essential for long-term rescue of a severe spinal muscular atrophy mouse model. Nature 2011; 478: 123–6.

Janzen E. Identification of binding partners of plastin 3, a modifier of spinal muscular atrophy [Master thesis]. Cologne, Germany: University of Cologne; 2013.

Kaifer KA, Villalon E, Osman EY, Glascock JJ, Arnold LL, Cornelison DD, et al. Plastin-3 extends survival and reduces severity in mouse models of spinal muscular atrophy. JCI Insight 2017; 2: e89970.

Kariya S, Park GH, Maeno-Hikichi Y, Leykekhman O, Lutz C, Arkovitz MS, et al. Reduced SMN protein impairs maturation of the neuromuscular junctions in mouse models of spinal muscular atrophy. Hum Mol Genet 2008; 17: 2552–69.

Kashima T, Manley JL. A negative element in SMN2 exon 7 inhibits splicing in spinal muscular atrophy. Nat Genet 2003; 34: 460–3.

Kong L, Wang X, Choe DW, Polley M, Burnett BG, Bosch-Marce M, et al. Impaired synaptic vesicle release and immaturity of neuromuscular junctions in spinal muscular atrophy mice. J Neurosci 2009; 29: 842–51.

Kuwahara H, Kamei J, Nakamura N, Matsumoto M, Inoue H, Kanazawa H. The apoptosis-inducing protein kinase DRAK2 is inhibited in a calcium-dependent manner by the calcium-binding protein CHP. J Biochem 2003; 134: 245–50.

Ladner CJ, Czech J, Maurice J, Lorens SA, Lee JM. Reduction of calcineurin enzymatic activity in Alzheimer's disease: correlation with neuropathologic changes. J Neuropathol Exp Neurol 1996; 55: 924–31.

Le Roy C, Wrana JL. Clathrin- and non-clathrin-mediated endocytic regulation of cell signalling. Nat Rev Mol Cell Biol 2005; 6: 112–26.

Lefebvre S, Burglen L, Reboullet S, Clermont O, Burlet P, Viollet L, et al. Identification and characterization of a spinal muscular atrophy-determining gene. Cell 1995; 80: 155–65.

Lin X, Sikkink RA, Rusnak F, Barber DL. Inhibition of calcineurin phosphatase activity by a calcineurin B homologous protein. J Biol Chem 1999; 274: 36125–31.

Liu J, Farmer JD Jr, Lane WS, Friedman J, Weissman I, Schreiber SL. Calcineurin is a common target of cyclophilin-cyclosporin A and FKBP-FK506 complexes. Cell 1991; 66: 807–15.

Liu Q, Fischer U, Wang F, Dreyfuss G. The spinal muscular atrophy disease gene product, SMN, and its associated protein SIP1 are in a

complex with spliceosomal snRNP proteins. Cell 1997; 90: 1013–21.

Liu Y, Zaun HC, Orlowski J, Ackerman SL. CHP1-mediated NHE1 biosynthetic maturation is required for Purkinje cell axon homeostasis. J Neurosci 2013; 33: 12656–69.

Lorson CL, Hahnen E, Androphy EJ, Wirth B. A single nucleotide in the SMN gene regulates splicing and is responsible for spinal muscular atrophy. Proc Natl Acad Sci USA 1999; 96: 6307–11.

Lunn MR, Wang CH. Spinal muscular atrophy. Lancet 2008; 371: 2120–33.

Macia E, Ehrlich M, Massol R, Boucrot E, Brunner C, Kirchhausen T. Dynasore, a cell-permeable inhibitor of dynamin. Dev Cell 2006; 10: 839–50.

McWhorter ML, Monani UR, Burghes AH, Beattie CE. Knockdown of the survival motor neuron (Smn) protein in zebrafish causes defects in motor axon outgrowth and pathfinding. J Cell Biol 2003; 162: 919–31.

Mendell JR, Al-Zaidy S, Shell R, Arnold WD, Rodino-Klapac LR, Prior TW, et al. Single-dose gene-replacement therapy for spinal muscular atrophy. N Engl J Med 2017; 377: 1713–22.

Mendoza-Ferreira N, Coutelier M, Janzen E, Hosseinibarkooie S, Lohr H, Schneider S, et al. Biallelic CHP1 mutation causes human autosomal recessive ataxia by impairing NHE1 function. Neurol Genet 2018; 4: e209.

Mentis GZ, Blivis D, Liu W, Drobac E, Crowder ME, Kong L, et al. Early functional impairment of sensory-motor connectivity in a mouse model of spinal muscular atrophy. Neuron 2011; 69: 453–67.

Miller N, Feng Z, Edens BM, Yang B, Shi H, Sze CC, et al. Non-aggregating tau phosphorylation by cyclin-dependent kinase 5 contributes to motor neuron degeneration in spinal muscular atrophy. J Neurosci 2015; 35: 6038–50.

Mourelatos Z, Dostie J, Paushkin S, Sharma A, Charroux B, Abel L, et al. miRNPs: a novel class of ribonucleoproteins containing numerous microRNAs. Genes Dev 2002; 16: 720–8.

Murray LM, Comley LH, Thomson D, Parkinson N, Talbot K, Gillingwater TH. Selective vulnerability of motor neurons and dissociation of pre- and post-synaptic pathology at the neuromuscular junction in mouse models of spinal muscular atrophy. Hum Mol Genet 2008; 17: 949–62.

Nolle A, Zeug A, van Bergeijk J, Tonges L, Gerhard R, Brinkmann H, et al. The spinal muscular atrophy disease protein SMN is linked to the Rho-kinase pathway via profilin. Hum Mol Genet 2011; 20: 4865–78.

Oprea GE, Krober S, McWhorter ML, Rossoll W, Muller S, Krawczak M, et al. Plastin 3 is a protective modifier of autosomal recessive spinal muscular atrophy. Science 2008; 320: 524–7.

Pang T, Su X, Wakabayashi S, Shigekawa M. Calcineurin homologous protein as an essential cofactor for Na+/H+ exchangers. J Biol Chem 2001; 276: 17367–72.

Pellizzoni L, Kataoka N, Charroux B, Dreyfuss G. A novel function for SMN, the spinal muscular atrophy disease gene product, in pre-mRNA splicing. Cell 1998; 95: 615–24.

Riessland M, Kaczmarek A, Schneider S, Swoboda KJ, Lohr H, Bradler C, et al. Neurocalcin delta suppression protects against spinal muscular atrophy in humans and across species by restoring impaired endocytosis. Am J Hum Genet 2017; 100: 297–315.

Roberts B, Pohl J, Gooch JL. A fluorimetric method for determination of calcineurin activity. Cell Calcium 2008; 43: 515–19.

Schreij AM, Fon EA, McPherson PS. Endocytic membrane trafficking and neurodegenerative disease. Cell Mol Life Sci 2016; 73: 1529–45.

Schreml J, Riessland M, Paterno M, Garbes L, Rossbach K, Ackermann B, et al. Severe SMA mice show organ impairment that cannot be rescued by therapy with the HDACi JNJ-26481585. Eur J Hum Genet 2013; 21: 643–52.

Shababi M, Lorson CL, Rudnik-Schoneborn SS. Spinal muscular atrophy: a motor neuron disorder or a multi-organ disease? J Anat 2014; 224: 15–28.

Smillie KJ, Cousin MA. Akt/PKB controls the activity-dependent bulk endocytosis of synaptic vesicles. Traffic 2012; 13: 1004–11.

Srinivasan S, Severa M, Rizzo F, Menon R, Brini E, Mechelli R, et al. Transcriptional dysregulation of interferome in experimental and human multiple sclerosis. Sci Rep 2017; 7: 8981.

Stanley JL, Lincoln RJ, Brown TA, McDonald LM, Dawson GR, Reynolds DS. The mouse beam walking assay offers improved sensitivity over the mouse rotarod in determining motor coordination deficits induced by benzodiazepines. J Psychopharmacol 2005; 19: 221–7.

Storbeck M, Hupperich K, Gaspar JA, Meganathan K, Martinez Carrera L, Wirth R, et al. Neuronal-specific deficiency of the splicing factor tra2b causes apoptosis in neurogenic areas of the developing mouse brain. PLoS One 2014; 9: e89020.

Sugarman EA, Nagan N, Zhu H, Akmaev VR, Zhou Z, Rohlfs EM, et al. Pan-ethnic carrier screening and prenatal diagnosis for spinal muscular atrophy: clinical laboratory analysis of >72 400 specimens. Eur J Hum Genet 2012; 20: 27–32.

Tan TC, Valova VA, Malladi CS, Graham ME, Berven LA, Jupp OJ, et al. Cdk5 is essential for synaptic vesicle endocytosis. Nat Cell Biol 2003; 5: 701–10.

Torres-Benito L, Ruiz R, Tabares L. Synaptic defects in spinal muscular atrophy animal models. Dev Neurobiol 2012; 72: 126–33.

Wirth B, Barkats M, Martinat C, Sendtner M, Gillingwater TH. Moving towards treatments for spinal muscular atrophy: hopes and limits. Expert Opin Emerg Drugs 2015; 20: 353–6.

Wirth B, Brichta L, Schrank B, Lochmuller H, Blick S, Baasner A, et al. Mildly affected patients with spinal muscular atrophy are partially protected by an increased SMN2 copy number. Hum Genet 2006; 119: 422–8.

Wirth B, Mendoza-Ferreira N, Torres-Benito L. Chapter 12—Spinal muscular atrophy disease modifiers. In: Sumner CJ, Paushkin S, Ko CP, editors. Spinal muscular atrophy. Amsterdam: Academic Press, Elsevier; 2017. p. 191–210.

Wu XS, Zhang Z, Zhao WD, Wang D, Luo F, Wu LG. Calcineurin is universally involved in vesicle endocytosis at neuronal and nonneuronal secretory cells. Cell Rep 2014; 7: 982–8.